STUDY OF MASS TRANSFER
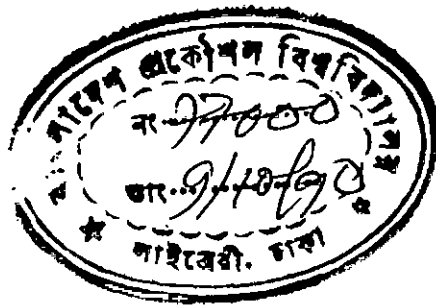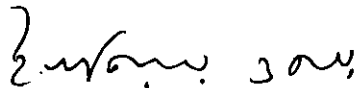# INFLUENCED BY GAS SPARGING
AND SIMULTANEOUS GAS-LIQUID
FLOW

SULATA MOJUMDER

BANGLADESH UNIVERSITY OF ENGINEERING AND TECHNOLOGY
DEPARTMENT OF CHEMICAL ENGINEERING
CERTIFICATION OF THESIS WORK

We, the undersigned, certify that <u>SULATA MOJUMDER</u> candidate for degree of <u>Master of Science in Engineering (Chemical)</u> has presented her thesis on the subject "<u>STUDY OF MASS TRANSFER INFLUENCED BY GAS SPARGING AND SIMULTANEOUS GAS-LIQUID FLOW</u>" that the thesis is acceptable in form and content, and that the student demonstrated a satisfactory knowledge of the field covered by this thesis in an oral examination held on August 18, 1990.
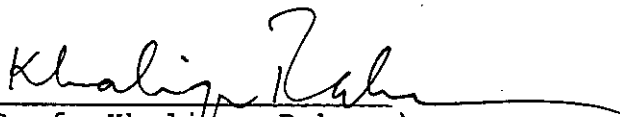

(Dr. Sabder Ali)
Associate Professor
Department of Chemical Engineering
Chairman, Examination Committee.

(Prof. K. Ikhtyar Omar)
Professor and Head
Department of Chemical Engineering
Member, Examination Committee.

(Mr. Ali Afzal Khan)
Chief Production Manager
Urea Fertilizer Factory Ltd. Ghorashal
External Member, Examination Committee.

(Prof. Khalilur Rahman)
Professor
Department of Chemical Engineering
Member, Examination Committee.

STUDY OF MASS TRANSFER INFLUENCED BY GAS SPARGING AND SIMULTANEOUS GAS-LIQUID FLOW

A THESIS

SUBMITTED TO THE DEPARTMENT OF CHEMICAL ENGINEERING

IN PARTIAL FULFILMENT OF THE REQUIREMENTS

FOR THE DEGREE OF

MASTER OF SCIENCE IN ENGINEERING (CHEMICAL)

BANGLADESH UNIVERSITY OF ENGINEERING AND TECHNOLOGY,DHAKA

BY

SULATA MOJUMDER
AUGUST,1990

ABSTRACT

The present work has been carried out in order to study rate of mass transfer by different modes of convection in a vertical parallel plate electrochemical reactor using copper electrodes. The modes of convection used were : (1) sparging of gas thorough stationary solution and (2) simultaneous gas and liquid flow. Current distributions and mass transfer rates under different hydrodynamic conditions within the cell were obtained by measuring currents at different sections of the cathode by employing the copper deposition reaction from acidified copper sulphate solution. Mass transfer data were generated by using the limiting current technique.

Correlations obtained for gas sparging through stationary electrolyte and simultaneous gas-liquid flow were $K_g \propto U_g^{0.4}$ and $K_{tp} = 2.08 \times 10^{-5}(U_g^{0.4}/U_l^{0.2})$ respectively. The results were also correlated with the average bubble diameter (Sherwood number and Reynolds number based on bubble diameter). These results have been compared with relevent previous works. Average mass transfer correlation was obtained for gas sparging through stationary solution.

An extensive literature survey of industrial electrochemical processes and electrochemical mass transfer in different forced convective systems has been included.

ACKNOWLEDGEMENTS

CONTENTS

APPENDICES

APPENDIX   A

Cell Dimension and Physical Properties of
Copper Sulphate in Sulphuric Acid Solution
and Other Relevant Data.

APPENDIX   B

Flow Calibration Curves for Rotameters
Used in the Experiments.

APPENDIX   C

Experimental Current-Voltage Data and
Calculated Results for Gas Sparging
Through Stationary Solution.

APPENDIX   D

Experimental Current-Voltage Data and
Calculated Results for Simultaneous
Gas-Liquid Flow.
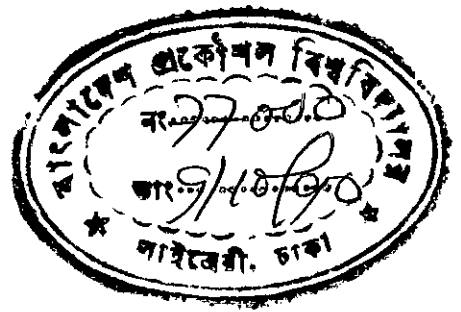
INTRODUCTION

Electrodeposition of metals from solutions are frequently useful industrial processes . There are several widely used methods of electrodeposition like electroplating,electrowinning and electrorefining.   In case where it is necessary to improve the chemical and physical properties of the material, thin surface layers of metal or metal substrate upon the material is produced using electroplating process. Electrowinning produces high purity metal from dilute and moderately concentrated solutions containing metal ions by electrodeposition, whereas electrorefining process involves the desired purity of metal by a combination of dissolution of an impure anode of the metal and deposition of pure metal at the cathode.   Another process involving metal deposition is electroforming and one important anodic process is electrochemical machining.

Efforts are being made to produce good quality even deposits and mass transfer studies of electrochemical processes are given special emphasis in this regard. Poor and uneven deposits occur mainly because of operating these above cathodic processes at high current

densities which gives a nonuniform mass transfer rate. Deposition at high current densities produces powderly deposits that are poorly adherent.

Ideally mass transfer should be intensive as well as uniform over the entire electrode surface. Generally operation at low current densities gives good quality deposits but the rate of mass transfer is not uniform over the whole of the electrode and locally high rates can cause poor electrodeposition. Well defined and controlled forced convection could give rise to increased and uniform rates of depositon.

The design of flow cells requires a thorough understanding of the mass transfer processes which largely govern the local current density and local potential. The systematic treatment of transport phenomena in chemical engineering has produced a solid basis for analyzing convective mass transfer in electrochemical reactors. Applying analogies between momentum, heat and mass transfer, electrochemical measurements provide insight into the fundamental nature of free and forced convection, specially for flow cells under laminar and turbulent flow conditions. These

2

are convenient for obtaining transport rate correlations which are useful for design purposes in nonelectrochemical systems as well.

As engineering studies of practical reactor designs increase in number, emphasis has changed from classical flow geometries , for which theoretical solutions are available to more specialised designs. Even so, the preferred engineering design is a parallel plate configuration due to ease of design, construction and maintenance as well as uniformity of current distributions under certain conditions. They provide a surface area to volume ratio second only to particulate cells a virtually equipotential system.Thus parallel plate electrochemical reactor has been used.

Experimental mass transfer data have mainly been obtained in systems with long hydrodynamic entrance and exit regions in order to ensure fully developed flow. The present work has been carried out to investigate the rate of mass transfer in the cathodic deposition of copper from acidified solutions of copper sulphate using two different modes of convection: 1) sparging of gas through stationary solution to agitate it and 2) simultaneous forced circulation of electrolyte and injection of gas at different flowrates. The result has been presented in .

engineering terms in order to relate them to electrochemical reactor design. This study possesses industrial importance also for electrorefining processes for anodic dissolution and for deposition from very low concentration of ions. In order to keep the limiting currents at low values and to cause slow dissolution of the anode, dilute solutions have been preferred. Since the cathodic reaction is mass transfer controlled, the use of sectioned cathode enables the current distribution and flow development to be studied by the limiting current technique.

A thorough review of relevent literature inclusive of a discussion of the theoretical principles partaining to the electrochemical system undertaken has also been presented. Results obtained from the experiments performed were presented, correlated and discussed as well as comparisons have been made between the present study and the relevent previous works.

LITERATURE ON ELECTROCHEMICAL MASS TRANSFER

2.1   INTRODUCTION

In this chapter the work done by previous workers in the field of mass transfer in parallel plate electrolytic cell under flow condition is reviewed. Most of the previous works had been confined to laminar and turbulent flows with very little reported on mass transfer in cells where gas sparging agitation or simultaneous gas-liquid flow had been used to produce convection.

2.2   MASS TRANSFER IN FLOW SYSTEM

Mass transfer in an electrochemical system under flow condition depends on the movement of ionic species, current flow, electroneutrality and the hydrodynamics of the system. The flux of any dissolved species or ions in dilute solutions is given by:

$$N_i = - Z_i\, D_i\, F\, C_i \nabla.\Phi - D_i \nabla.C_i + C_i\, U \ \dots\ (2.1)$$

where N_i is the molar flux of the species i

Z_i is the valency of the species i

C_i is the concentration of the species i

Φ is the electrostatic potential

D_i is the diffusion coefficient of i

U is the velocity of the electrolyte

F is the Faraday constant.

For flow systems, equation (2.1) has to be considered along with hydrodynamics and material balance of the system to obtain a complete solution. A material balance for a species i for a small volume of reactor with no chemical reaction in the bulk leads to a differential conversation law:

$$\delta C_i/\delta t = - \nabla.N_i \quad \ldots\ldots\ldots\ldots\ldots \quad (2.2)$$

where t stands for time.

At steady state, the concentration C is independent of time so that $\delta C_i/\delta t = 0$. Moreover in a system where excess of indifferent electrolyte is present, the ionic migration term in equation (2.1) can be neglected. So we have the steady state diffusion equation of the form:

$$U. \nabla.C_i = D_i \nabla.^2 C_i \quad \ldots\ldots\ldots\ldots\ldots \quad (2.3)$$

Equation (2.3) can be rewritten as:

$$U_x(\delta C_i/\delta x)+U_y(\delta C_i/\delta y)+U_z(\delta C_i/\delta z)$$
$$=D_i(\delta^2 C_i/\delta x^2 +\delta^2 C_i/\delta y^2 +\delta^2 C_i/\delta z^2)\ldots\ldots(2.4)$$

For a complete solution equation (2.4) must be combined with the equation of continuity and Navier Stoke's equation which describe the fluid velocity distribution.

2.3 GAS SPARGING IN STATIONARY SOLUTION

For electrodeposition of metal, electroplaters have long used open-topped vats which are agitated by the introduction of air from a pipe at the bottom of the tank. Such stirring is relatively ineffective since the electrode gaps are wide from 0.02 m to 0.05 m. Large submarine batteries have been fitted with air spargers to reduce the polarisation at very high discharge rates. For the electrolytic recovery of photographic fixing solution, a narrowly spaced vertical parallel plate cell with air sparging has been used, but the air bubbles created problems as they tended to polarise the silver cathode and reduce its effective area and caused foaming at the top of the cell.

All the above processes had problems caused by incorrect electrode spacing and a too high air flow rate. To understand these problems a quantitative and qualitative discussion of mass transfer enhancement by gas sparging has been presented.

2.3.1 QUALITATIVE DESCRIPTION OF MASS TRANSFER ENHANCED BY GAS SPARGING

There is little relevant literature dealing with the enhancement of mass transfer at an electrode surface when stationary solution is agitated by gas sparging. The experimental study and qualitative treatment made by Grendron and Ettel (1975) as well as Ali (1982) will be outlined here. They investigated the performance of a copper electrowinning cell with a view to produce high quality cathodes at significantly higher current densities and compared gas sparging with different methods for enhancement of mass transfer. Grendron and Ettel used a method which enabled measurement of local values of the cathode mass transfer co-efficient under any operating conditions. This method was based on the mass transfer controlled co-deposition of silver added to the electrolyte in a tracer concentration. By analyzing the cathode deposit and the silver concentration of the electrolyte, they calculated the cathode mass transfer co-efficient for silver ions as well as copper ions using hydrodynamic theory.

Using the above method, Ettel and Grendron constructed horizontal and vertical maps of the cathode mass transfer coefficient in a model cell having the same height as a full scale with different methods for achieving

8

convective mass transfer was adopted.

When natural convection with gas evolution takes place in a full height cell model, the upward flow of electrolyte at the anode is driven by anodically generated oxygen. The electrolyte in the upper half of the cathode is characterized by random turbulent flow which increases the mass transfer co-efficient (1.5×10^{-5} m/s) substantially. The bottom part of the cathode is operating under natural convection conditions. The agitation caused by the anodic gas results in high mass transfer coefficients compared to those where natural convection predominates (0.5×10^{-5} m/s). The bottom part of the cathode produced convectional flat anodes which were substantially rougher than the top parts due to higher cathode overpotential and lower limiting current at the bottom.

By employing a fast recirculation of electrolyte through the orifices from beneath the electrodes upwards to the cathode, a two-dimensional map of the local values of cathode mass transfer coefficient shows that it is substantially increased only in the viscinity of the electrolyte near jetting position (1.6×10^{-5} m/s). At the central and upper positions of the cathode the mass transfer coefficient had similar values to those obtained

in natural convection with gas evolution (i.e. 0.75×10^{-5} m/s at the outlet). The turbulence produced near the orifice is rapidly damped in the narrow space between the electrodes.

Circulation of the electrolyte between the electrodes resulted in a significant increase in mass transfer co-efficient. Moderate values of mass transfer co efficient (2.2×10^{-5} m/s at Reynolds number of 28000) were achieved in laminar and turbulent flow regime but this would result in very high pumping costs.

Agitation using gas sparging by means of a PVC tube sparger with 1 mm diameter hole at 5 mm pitch over the face of the cathode, the cathodic mass transfer is increased. They used an electrolyte containing 0.95 M copper sulphate in 1.25 M sulphuric acid solution at a current density of 1000 A/m^2 over an electrode area of 0.15 m^2 (1 m in length and 0.15 m in width) at 55° C. The air flowrate was varied from 0.00034 m^3/(m^2)(min) or 1.7 lit/min to 0.034 m^3/(m^2)(min) or 17 lit/min which resulted in an increase in mass transfer coefficient from 2.0 to 3.5×10^{-5} m/s. The effect of reducing the electrode spacing from 0.005 m to 0.002 m at 0.034 m^3/(m^2)(min) resulted in an increase in mass transfer coefficient from 3.0×10^{-5} to 4.5×10^{-5} m/s. From the hydrodynamic patterns

10

in horizontal and vertical mapping under natural and forced convection in an electrochemical reactor , they concluded that gas sparging is the superior method of agitation since it can provide high and fairly uniform turbulence over the entire cathode surface with high values of mass transfer coefficients.

Recently Ali (1982) used a rectangular vertical electrolytic cell with diffuser and reducer respectively at the inlet and outlet sections of the cell in order to minimize sudden expansion and contraction effects. Moreover he used a gas sparger connected to the diffuser having 1 mm diameter holes on a pitch of 5 mm and this gave a mass transfer coefficient of $2.944\ 10^{-5}$ to $8.060\ 10^{-5}$ m/s keeping electrode spacing at 0.002 m.

2.3.2 EFFECT OF GAS SPARGING ON THE ELECTROLYTE CONDUCTIVITY

A number of workers have studied the change of the effective conductivity of electrolyte due to the presence of gas bubbles . Maxwell (1881) was the first to derivea theoretical correlation of effective conductivity of two phase dispersion containing a random suspension of spherical particles of uniform diameter. He assumed that the average distance between the particles was large

enough so that the electric field around an individual particle was not disturbed by the presence of other particles. This condition is only true when void fraction(f) tends to zero.

Maxwell's equation is:

$$k_{g1}/k_1 = \{k_d + 2k_o - 2f(k_1 - k_d)\}/\{k_d + 2k_o + f(k_1 - k_d)\} \ldots (2.5)$$

where k_{g1} is the conductivity of two phase dispersion, k_1 is the conductivity of gas free solution and k_d is the conductivity of the dispersed phase.

De La Rue and Tobias (1959) estimated that equation (2.5) is satisfactory only for dilute dispersions of void fraction less than 0.25 because at f=0.25 the average distance between the spherical particles was about 30% of the particle diameter and the electric field around the spheres is markedly distorted. Equation (3.1) should not be applicable for void fraction f>0.2.

Numerous attempts have been made to approximate equation (2.5) to estimate the effective conductivities in concentrated suspension. One such approximation was made by Raleigh (1984) who considered k_d to be very small compared to k_1 as for gas bubbles in an electrolyte. Equation (2.5) can be simplified:

$$K_{g1}/K_1 = (1-f)/(1+f/2) \ldots \ldots (2.6)$$

The values of the conductivity ratio for mixed sized bubbles having a large bubble size range agrees reasonably well with Bruggemann's treatment (1935). Bruggemann considered that if large spherical particles were added to a dispersion containing much smaller particles, the disturbance of the field around the large particles due to the small spheres could be considered negligible. On this the effective conductance (relative conductivity) of such a system may be evaluated by considering the surroundings of the large sphere to be a continuum and then applying Maxwell's equation, since the system is dilute as far as the large sphere is concerned. Bruggemann's correlation for nonconductivity phase, i.e. for gas bubbles when $k_d = 0$, is

$$k_{g1} / k_1 = (1-f)^{3/2} \qquad \ldots\ldots\ldots\ldots\ldots(2.7)$$

For narrow bubble size ranges , the value of relative conductivity lies between Bruggemann's and Maxwell's correlation. De La Rue and Tobias pointed out that although the Maxwell correlation should be valid only at low values of f and k_{g1} / k_1, the experimental results agree well upto f=0.6. Siggrist et el (1980) also concluded that Maxwell's correlation was superior to Bruggemann's in the case of gas bubbles in moderately concentrated electrolytes where the bubble size ranges are narrow and to be valid upto f=0.6. In practice the value of gas voidages do not exceed f=0.15 and a

linearised form of equations (2.6) or (2.7) can be used
where the equations reduce to a simple form:

$$K_{g1}/K_1 = 1 - 1.5 \ f \qquad \ldots\ldots\ldots\ldots(2.8)$$

Equation (2.8) can be used upto gas void fraction
of about 0.12.

2.3.3 THE FORMATION AND SIZE RANGE OF BUBBLES PRODUCED BY AN AIR SPARGER

A lot of workers have studied the formation of bubbles
at an orifice immersed in a liquid. The principal factors
which affect the diameter of bubbles produced at an
orifice are many, but their sizes are primarily affected
by:

1. The orifice, its diameter, the shape, the
submergence, angle of inclination and the flow
condition of liquid near the orifice.

2. Liquid inertia effect.

3. Liquid density.

4. Liquid viscosity.

5. Static and dynamic surface tension of liquid.

6. The relationship between the constancy of gas flow
   and the constancy of pressure at the orifice.

There are three regimes of bubble formation:single bubble
(at low gas flow rate), intermediate (laminar) and jet
(turbulent) regimes. Considering the forces acting on

14

each bubble during its formation, the bubble is acted
upon by buoyancy, the convection currents in the fluid,
and by the surface tension forces acting on the section
of the bubble that is still in contact with the orifice.
For low gas flow rates, when the viscosity of the liquid
is small and convection is negligible, the bouyancy and
surface tension forces approximately balance and assuming
the bubbles spherical, the forces are given by:

$$(1/6) \ \pi \ d_B{}^3 \ g \ (\ \rho_1 - \rho_g) = \pi \ d_o \ \sigma \ \ldots\ldots(2.9)$$

where d_B is the bubble diameter; g is the acceleration
due to gravity; ρ_1 is the liquid density; ρ_g is the
density of gas; d_o is the orifice diameter; σ is the
surface tension; from which:

$$d_B = \{ \ 6 \ d_o \ \sigma \ / \ g \ (\ \rho_1 - \rho_g)\}^{1/3} \qquad \ldots.(2.10)$$

Equation (2.10) can be rewritten as:

$$d_B/d_o = C(\ 4\sigma/g \ (\ \rho_1 - \rho_g) \ d_o{}^2)^{1/3} \ \ldots..(2.11)$$

The value of constant C should be $(1.5)^{1/3} = 1.15$ but
experimental work has shown that the value of C is around
unity.

For low gas flowrates, another correlation is also
applicable, which is:

$$V_B = \ \psi_H \ d_o\sigma/(\ \rho_1 - \rho_g) \ g \qquad \ldots\ldots..(2.12)$$

where ψ_H is the Harkin factor, and Harkin's factor can
be written (for $0 \leq d_o/V_B{}^{1/3} \leq 0.6$) as:

$$\psi_H = 1.000 - 0.66023 d_o/V_B{}^{1/3} + 0.3395 d_o{}^2/V_B{}^{2/3} \qquad (2.13)$$

15

The volume of gas bubble can be calculated from equation (2.13). As the gas flow is increased the frequency of bubble formation increases but the bubble size remains constant upto an orifice Reynolds number of 200. As the flowrate is increased further, between orifice Reynolds number of 200 and 2100 (laminar or intermediate regime), the frequency of bubble formation becomes approximately constant but the bubble diameter increases with gas flowrate. At higher flows (Re_o > 2100), there is a considerable range of bubble sizes with a production of numerous small bubbles due to bubble break up in the turbulent regime instead of a single bubble size. This transition point cannot be regarded as a sharp one because a certain degree of bubble break up may take place at lower Reynolds number. Between the two regimes there is a range of gas flowrate over which the bubble size decreases with the increase in air flowrate, owing to the establishment of liquid current that nips the bubbles off prematurely.

In Reynolds number range of 200 < Re_o <21000, the bubble size becomes mainly dependent on viscous and inertial forces rather than the surface tension force or the momentum of the issuing gas. For the air/water system, Leibson (1956) suggested the following correlation:

$$d_B = 0.0287 \ d_o^{1/2} \ Re_o^{1/3} \qquad \ldots (2.14)$$

In this region the bubbles form in drains rather than seperately. Ramkrishnan et el (1969) proposed that bubble formation takes place in two stages, expansion when the bubble remains attached to the orifice and detachment when the bubble moves away from the orifice, keeping in contact with the orifice through a 'neck'.

With the further increase in air flow, turbulence occurs at the orifice and the gas stream approaches the appearance of a continuous jet which breaks up at 8 to 10 cm above the orifice. The stream contains the large, closely spaced, irregular bubbles consisting of spherical caps and toroidal shape with a rapid swirling motion. At higher flowrates the proportion of toroidal bubbles increases and breaks up rapidly but the spherical cap bubble has a relatively stable configuration. Leibson et el (1956) measured the average bubble size by a photographic method and found a sharp fall over the Reynolds number 2100 to 10000 from the laminar values, which is given by:

$$d_{vs} = 0.0071 \, Re_o^{-0.05} \qquad \ldots\ldots\ldots(2.15)$$

where d_{vs} is the volume surface diameter of the bubble and is in metres. This equation has been confirmed by other workers. At higher Reynolds number the bubble size is independent of orifice diameter.

Equation (2.15) can be applied for the determination of bubble sizes formed at the multiple orifices, but at high velocities coalescence of bubbles formed at individual orifices occurs. The bubble sizes depend on other factors such as bubble rise through liquid and its flow condition and other restrictions in the way of rising bubbles.

2.3.4 MASS TRANSFER ENHANCEMENT BY GAS EVOLUTION

The evolution of gas at electrode surface promotes mass transfer rates and for a given spacing between the electrodes the rates of mass transfer will be increased as the the rate of gas production increases. For a given current density at an electrode, the rate of mass transfer will be increased by a reduction in spacing between the electrodes due to increased circulation of electrolyte. If the gas is evolved at the electrode surface the mass transfer rates are much higher because the diffusion layer is periodically destroyed when the bubbles detach themselves from the interface.

Venczel (1961) measured the rate of mass transfer of Fe^{3+} or Ce^{4+} ions in sulphuric acid at different metal electrode evolving hydrogen and obtained the expression:

$$\delta \propto (V_g/A_e)^{-m} \qquad \ldots\ldots\ldots\ldots(2.16)$$

where δ is the thickness of diffusion layer

V_g is the rate of gas evolution

A_e is the electrode area

m is a factor dependent on current density.

Evidently the exponent m also depends on the special experimental device and is influenced by the convective flow. Equation (2.16) is an empirical correlation for mass transfer due to gas evolution which can be rewritten in the form:

$$K \propto (V_g/A_e)^m$$

$$K \propto D (V_g/A_e)^{m} \qquad \ldots\ldots\ldots\ldots (2.17)$$

where K is the mass transfer coefficient; D is the diffusion coefficient of the involved species; the value of m has been confirmed by a lot of workers as 0.5, but Roald and Beck (1951) put the value as 0.59 and according to Kind (1975) it varies between 0.45 and 0.66. Ibl (1971) studied the enhancement of mass transfer by gassing at electrodes in static solution whose diffusion layer thickness was between 2×10^{-5} m to 2×10^{-4} m and obtained the correlation as:

$$K = D (V_g/A_e)^{0.5}/(1.5 \times 10^{-6}) \qquad \ldots\ldots\ldots (2.18)$$

Janssen and Hooghland (1970) found that the thickness of diffusion layer decreases with increasing current density in the case of hydrogen and oxygen evolution, this decrease being marked for i > 2000 A/m^2. They also found

that the thickness of diffusion layer increases along the height of the electrode according to:

$$\log \delta = a_i + 0.13 \log x_i \quad \ldots \ldots (2.19)$$

where a_i depends on current density, increasing with decreasing value of i, and x_i is the distance from the leading edge of the electrode. From experimental data, they found the value of exponent m varies from 0.36 to 0.71.

Sedahmed (1978) studied mass trnsfer on the electro-deposition of copper from an acidified copper sulphate solution at an array of closely packed screen stirred by oxygen and found the value of m = 0.38. He compared the results with other systems stirred by evolved gas and the value of m in those studies was between 0.27 and 0.37. Mohanta and Fahidy (1977) studied the effect of bubble formaiton at the anode, due to the discharge of an anion, on the ionic mass transfer rate at the associated cathode. they found that when the bubbles were permitted to rise freely in the entire reactor, the cathodic mass transfer rate (Sh_g) was seen to incrase with respect to its magnitude observed under restricted conditions by placing copper baffle plate between the electrodes. The magnitude of this effect can be related as :

$$Sh_g = Sh_B + 3.008 \, Re_g^{0.77} \, Sc^{1/3} \, (h/s)^{0.336} \quad \ldots (2.20)$$

where $Re_{g,}$ is the Reynolds number of gas.

h is the height of the electrode

s is the spacing between the electrodes.

The relative incrase in the cathode mass transfer rate due to gas evolution (Sh_g) was not more than 20% with respect to the case of restricted bubble motion (Sh_B)

Stephan and vogt (1979) presented a mathmatical model approximately representing the real mass transfer processes at gas evolving electrodes and they obtained the correlation as:

$$Sh_g = 0.93 \ Re_A{}^{0.5} \ Sc^{0.487} \qquad \ldots\ldots\ldots\ldots(2.21)$$

where $Re_A = (V_g/A_e).(d_B/Y)$ and $Sh_g = Kd_B/D$

where d_B is the bubble diameter. Vogt (1978) also used analogical correlation for heat transfer in neucleate boiling,

$$N_u = 0.93 \ Re^{0.5} \ Pr^{0.487} \qquad \ldots\ldots\ldots(2.22)$$

Equations based on theoretical concept were developed by Ibl (1971). His equations are based on the assumption that mass transfer is governed by transient diffusion in quiescent liquid, which itself replaces the bubble immediately after the bubble breaks off so that liquid with bulk concentration touches the electrode. His experimental results can be correlated as:

$$Sh_g = (3.385/a) \ (Re_A \ Sc)^{0.5} \ (1-\theta)^{0.5} \ldots.(2.23)$$

where a is constant and the value of a = 2.0 for spherical and a = $4^{1/3}$ for semispherical bubbles; θ is the fractional surface coverage on the electrode by bubbles.

It would be resonable to consider the fractional surface coverage as void fraction of the bubble in the case of gas sparging and equation ((2.23) can be written as:

$$Sh_{dB} = (3.385/a)(Re_{dB} \ Sc)^{-0.5} \ (1-f)^{0.5} \qquad (2.24)$$

where $Sh_{dB} = K_g d_B/D$ and $Re_{dB} = u_g \ d_B/Y$

where K_g is the liquid phase mass transfer coefficient during gas sparging at stationary electrolyte; u_g is the superficial gas velocity.

2.4 TWO PHASE FLOW

Air agitation is one of the best methods of enhancing mass transfer in stationary solution, and the recirculation of electrolyte in turbulent conditions also improves the mass transfer rate for the deposition of copper at the cathode. A combination of both the processes will be briefly described . For electrochemical systems the preferred flow pattern is bubbly or homogenous flow regime because small bubbles will stir uniformly the electrolyte to yield uniform at the electrode surface.

22

2.4.1 GAS EVOLUTION IN FLOW SYSTEM

When gas evolution occurs in a flow electrochemical reactor, the situation becomes complex, since the flowing electrolyte will force the gas bubbles out of the diffusion layer which would result in a variation of current density along the electrode surface. Beck (1969) proposed that in a situation where combined effects operate, the overall mass transfer for gas evolution in electrolyte flow should be the addition of mass transfer coefficients calculated seperately:

$$1/\delta_{eff} = 1/\delta_1 + 1/\delta_2 \qquad \ldots\ldots\ldots (2.25)$$

where δ_{eff} is the diffusion layer thickness when both modes operate together. δ_1 and δ_2 relate to diffusion layer thickness that would be found in enhancement mode that operated singly.

Equation (2.25) could be expressed another way:

$$\beta = \beta_1 + \beta_2 \qquad \ldots\ldots\ldots\ldots\ldots\ldots\ldots\ldots\ldots (2.26)$$

and $\qquad i_{lim\ total} = i_{lim(1)} + i_{lim(2)} \qquad \ldots\ldots (2.27)$

where β is the overall mass transfer rate , β_1 and β_2 for individual mode of mass transfer for liquid and gas respectively.

Under laminar conditions the hypothesis of Beck agrees

quite well with the experimental data and the sum of i_{lim} (forced convection) and i_{lim} (gassing) ; but for the turbulent flow the limiting current is in good agreement with the gassing data only, calculated from Ibl's findings in equation (2.18).

Vogt (1978) adopted an equation of mass transfer rate in the reactor for turbulent flow with gas evolution as:

$$\beta = \beta_1 [1 + (\beta_2/\beta_1)^2]^{1/2} \qquad \ldots\ldots(2.28)$$

2.4.2   GAS- LIQUID ADSORPTION IN TWO PHASE FLOW

The gas liquid adsorption for two phase flow has been dealt with in section 2.3 which covers most of the literature survey of this section , but some aspects of two phase flow will be dealt with here. The gas liquid adsorption includes the adsorption and desorption of carbon dioxide by air from water in columns with sieve plate , grid tray or bubble cap tray , rectification of binary mixture and chemisorption oxidation of sulphate into sulphite. Most of the literature reveals the mass transfer coefficient for liquid phase depends on the superficial of gas and the correlation can be written as:

$$K_L \propto u_g^m \qquad \ldots\ldots\ldots\ldots(2.29)$$

where the value of exponent m varies from 0.14 to 1.19 but the value is mostly around 0.5.

24

Kasturi and Stepanek (1974) studied mass transfer rate in concurrent gas liquid flow through a vertical tube by absorbing sulphur dioxide into sodium hydroxide and carbon dioxide into sodium carbonate and sodium bicarbonate respectively. Both the liquid and gas phase mass transfer coefficient in upward flow increase with gas velocity. In the lower range of flow rates, increase in liquid velocity has a favourable effect on mass transfer coefficients, but a decrease in mass transfer results at high liquid flow rate due to increased entrainment of liquid. The liquid phase mass transfer rate can be expressed as:

$$Sh_L = 0.25 \ Sc_L^{-1/2} \ Pe_L \ Eu_L \qquad \ldots \ldots \ldots (2.30)$$

where Eu_L is the liquid Euler number.

Though the experimental study of gas liquid adsorption in two phase flow is not directly related to the present study, it can be reasonably applied for comparison purposes.

2.4.3 MASS TRANSFER IN GAS – LIQUID SYSTEMS

Mass transfer between gas and liquid will be briefly described because mass transfer in liquid phase is increased by the increase in air flow which has a close similarity to the study of electrochemical mass transfer,

25

that is mass transfer rate at the electrode surface increases from the agitation of elctrolyte by gas bubbles. Secondly, the mass transfer correlation for gas-liquid process is based on the fact that it occurs at the boundary layer of bubbles or from the surrounding liquid. It is possible that a fraction of bubbles may be moving close to the electrode surface whose boundary layer may coincide with the surrounding liquid near the electrode surface and then the mass transfer correlation for gas liquid processes can be used.

The governing equations which form the basis of mass transfer from single bubbles are:

1. Equation of continuity:

$$\delta u' \Upsilon'/\delta x' + \delta v' \Upsilon'/\delta y' = 0 \quad \ldots\ldots\ldots (2.31)$$

2. The equation of convctive diffusion in the boundary layer of bubbles for the continuous phase can be written as:

$$u'(\delta c'/\delta x') + v'(\delta c'/\delta y') = (2/Pe).(\delta^2 c'/\delta y'^2) \quad (2.32)$$

The prime on all quantities indicate the dimensionless coordinates and this is used where the thickness of the hydrodynamic boundary layer is much less than the equivalent radius of the bubbles, Υ', which can be expressed as:

$$u' = u/U \ , \ v' = v/U \ , \quad Y' = Y/Y_e \quad ,$$

$$x' = x/Y_e \ , \ y' = y/Y_e \ , \ C' = C/C_{eq}$$

where u is the tangential velocity component; v is the radial velocity component; U is the relative or superficial velocity; Y is the radial dimension; x and y are the corresponding linear dimensions parallel and perpendicular to the bubble surface respectively; C is the local concentration. C_{eq} is the equivalent concentration.

If the thickness of diffusion boundary layer is less than the thickness of the hydrodynamic boundary layer, mass transfer will occur in a region where the tangential velocity to the bubble surface is:

$$u' = u_o' + \beta_1 y \qquad \ldots\ldots\ldots\ldots\ldots (2.33)$$

where u_o' is a measure of the relative motion in the interior of the bubble; β_1 is the velocity gradient at the boundary layer.

Combining equation (2.32) and (2.33), and taking the prime off, it can be written as:

$$(u_o + \beta_1 y) \delta c / \delta x (1/Y)(\delta/\delta x)[(u_o y + 0.5 \beta_1 y^2)] \delta c / \delta y$$

$$= (2/Pe)(\delta^2 c / \delta y^2) \quad \ldots (2.34)$$

27

Equation (2.34) can be solved wtih the boundary conditions:

$C = 1$; $y = 0$

$C \rightarrow 0$; $y \rightarrow \infty$

The solution of the convective diffusion equation (2.34) for mobile, interface yeilds (assuming no flow seperation):

$$Sh_{dB} = 0.62 \ Re_{dB}^{1/2} \ Sc^{1/3} \qquad \ldots \ldots (2.35)$$

In practice, for the Reynolds number considered, flow seperation occurs at $108^{o}C$ so that mass transfer occuring over the surface of bubble upstreem of the seperation point is given by:

$$Sh_{dB} = 0.56 \ Re_{dB}^{1/2} \ Sc^{1/3} \qquad \ldots \ldots \ldots (2.36)$$

Equations (2.35) and (2.36) are common forms of mass transfer in a liquid system, but a radial diffusion term is added and it can be written in general form as:

$$Sh = 2.0 + b_1 \ Re_{dB}^{1/2} \ Sc^{1/3} \qquad \ldots \ldots \ldots (2.37)$$

Equation (2.37) was first proposed by Frossling (1938), based on the evaporation experiment in hot air streams and found b_1 . Other workers found a larger value of b_1. Rowe, Claxton and Lewis (1965), after a careful study over a Reynolds number from 30 - 2000, found the valuesof b_1 for air of 0.6 and for water $b_1 = 0.79$. When the interface velocity is of the same order as the mainstream velocty , the convective diffusion equation (2.34) can be solved for Re >> 1.

The mass transfer correlations for bubbles moving at high Reynolds number can be derived by the theoretical analysis of the boundary layer. Chao (1962) used a perturbation method to express the velocity fields inside and outside the mobile bubble moving at high Reynolds number and without flow seperation in the form of small deviation from the potential fields. The mass transfer correlation in this case is:

$$Sh_{dB} = 2/\sqrt{\pi}[1 - 2.96/Re_{dB}^{1/2}]Pe_{dB}^{1/2} \quad \ldots\ldots(2.38)$$

where $Pe_{dB} = Re_{dB}.Sc$.

When the Reynolds number is very high , equation (2.38) reduces to:

$$Sh_{dB} = 1.128 \ Pe_{dB}^{1/2} \quad \ldots\ldots\ldots\ldots(2.39)$$

which is the well known Bousinesq's solution for mass transfer around spheres in potential flow.

Equation (2.37) has been modified by Hughmark (1967) to correlate the data for a single bubble in liquid and liquid drops in liquid, as well as mass transfer to flowing air and liquid . The modified equation is of the form:

$$Sh_{dB} = 2+a_2[Re_B^{0.484} \ Sc^{0.339}(d_Bg^{1/3}/D_L^{2/3})^{0.072}]^{b_2}$$

$$\ldots\ldots\ldots\ldots(2.40)$$

for single gas bubbles $a_2 = 0.061$, $b_2 = 1.61$.

Generally bubble columns operate with swarms of bubbles rather than a single bubble, and the values of constants are $a_2 = 0.0187$ and $b_2 = 1.61$. Equation (2.40) can be rewritten as:

$$Sh_{dB} = (K_g d_B / D) =$$
$$2 + 0.0187 \ Re_s^{0.779} \ Sc^{0.545} (d_B \ g^{1/3} / D_L^{2/3})^{0.116} \qquad (2.41)$$

where D_L is the liquid diffusivity coefficient and Re_s is based on the slip velocity which can be expressed as:

$$Re_s = d_B \ u_s / \gamma_L \qquad \ldots \ldots \ldots \ldots (2.42)$$

where γ_L is the liquid kinematic viscosity and u_s is the slip or relative velocity between gas and liquid for upward flow of gas and liquid which can be defined as:

$$u_s = u_g / f - u_1 / (1 - f) \qquad \ldots \ldots \ldots (2.43)$$

where u_1 is the liquid superficial velocity. When the liquid is stationary, equation (2.43) becomes:

$$u_s = u_B = u_g / f \qquad \ldots \ldots \ldots \ldots \ldots (2.44)$$

where u_B is the bubble rise velocity.

Calderbank (1959) was the first to determine the bubble specific areas, the volumetric mass transfer coefficients and was able to calculate mass transfer coefficient. From experimental data for a number of gases both inorganic and organic, in water, glycol and glycol water mixture, he correlated the results as :

$$Sh_{dB} \ \propto \ (Re_g)^{0.776} \ Sc^{1/2} \qquad \ldots \ldots (2.45)$$

$$\text{and} \ \ Re_g = d_B \ u_t / \gamma_L$$

where u_t is the air bubble terminal velocity. The bubble size in the above experimental study varied from 0.002 m to 0.005 m.

2.4.4 MASS TRANSFER IN TWO PHASE FLOW ELECTROCHEMICAL REACTOR

Jennings et el (1975) studied mass transfer in parallel plate reactors (cross sectional area of 0.7 cm   14 cm = 9.8 cm²) whose electrodes were in horizontal position (area 100 cm²) for the deposition of copper ion (Cu^{2+}) from a solution of 100 ppm copper sulphate in 1 M sulphuric acid with two phase gas-liquid flow. Nitrogen was passed through a manifold consisting of 10 holes (2 mm dia) spaced at 1 cm intervals, and the gas flow rate was varied from nil to 14.5 l/min at an only constant flow rate of liquid of 4.5 l/min (7.8 cm/sec). They determined the experimental value of mass transfer coefficient j/C_o from the relationship of change in (i.e. reduction of) copper sulphate concentration with time upto electrolyte concentration of 25 ppm and interpreted j/C_o in terms of Prandtl-Taylor hypothesis of complete cessation of turbulence in the viscous sublayer and Levich-Landau hypothesis of gradual damping of turbulence in the viscous sublayer; they obtained the correlation as:

$$j \: / \: C_o \propto (\: u_1 + u_g \:) \qquad \ldots\ldots\ldots\ldots(2.46)$$

This shows the mass transfer enhancement results mainly from the increase in linear velocity of the liquid phase due to reduction of the effective cross sectional area of the cell caused by bubbles.

A study of mass transfer at vertical gas sparged electrodes, with or without superimposed electrolyte flow, has been carried out by Sigrist et el (1979) employing the well known limiting current method with electrolyte system Fe $(CN)_6^{-3}$ / Fe $(CN)_6^{-4}$. Nitrogen was introduced at the bottom of the reactor through vertical parallel plates at varied spacing of 1,2 and 4 cms apart, and the gas flow rate was varied between 0.17 and 0.82 $cm^3 cm^{-2} s^{-1}$, while the liquid flowrate was between 1.5 and 35.5 cm/s.

For a constant liquid flowrate the mass transfer coefficient for two phase flow, K_{tp} , increase in air flow but their values lie below the value of mass transfer coefficient of gas sparging through stationary solution. For a constant gas flow, K_{tp} decreases with the increase in liquid flow. From the experimentally observed relationship between void fraction, the gas and electrolyte superficial velocities, they found void fraction on u_g and u_l in a similar way as the mass transfer coefficient K_{tp} . They obtained the following

32

correlation from the experimental data as:

$$Sh = 0.19 \ (Ar^*.Sc)^{1/3} \quad \ldots\ldots\ldots(2.47)$$

where Ar* is the modified Archimedes number based on void

fraction and it can be expressed as:

$$Ar^* = (\ l^3g/ \ \gamma^2 \ ).(\ f/(1 -f)) \quad (2.48)$$

EQUIPMENT AND EXPERIMENTAL PROCEDURE

3.1   **INTRODUCTION**

A number of experiments were conducted with a vertical parallel plate cell having copper electrodes using 0.015M copper sulphate in 1.5M sulphuric acid as the electrolyte. The copper-copper sulphate system was preferred because unlike similar systems it is stable and insensitive to light, the cathodic reaction is mass transfer controlled, has been used by previous workers and has direct applicability to the existing electrochemical process. The cathode was sectioned to enable current measurements to be made at various sections along its length and this enabled mass transfer rates at different positions in the cell to be determined. The system was operated in two modes, namely,

1.   Passing gas bubbles through stalinary electrolyte through the cell
2.   Forced circulation of electrolyte with simultaneous flow of gas bubbles through the cell.

The gas used in the experiments was purely nitrogen (free of oxygen). The physical properties of this gas are
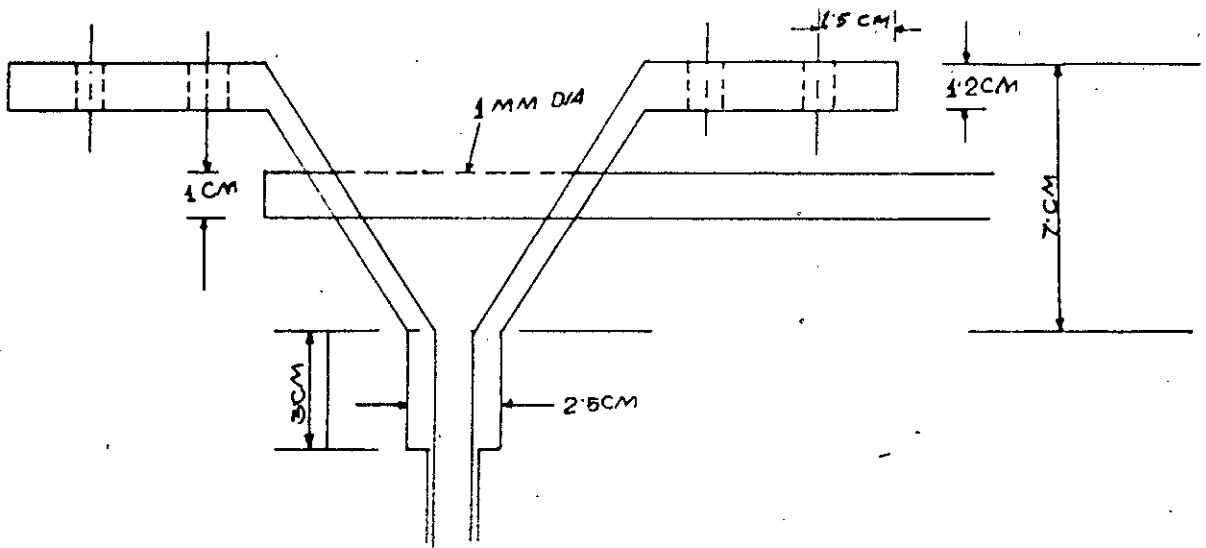
FRONT VIEW
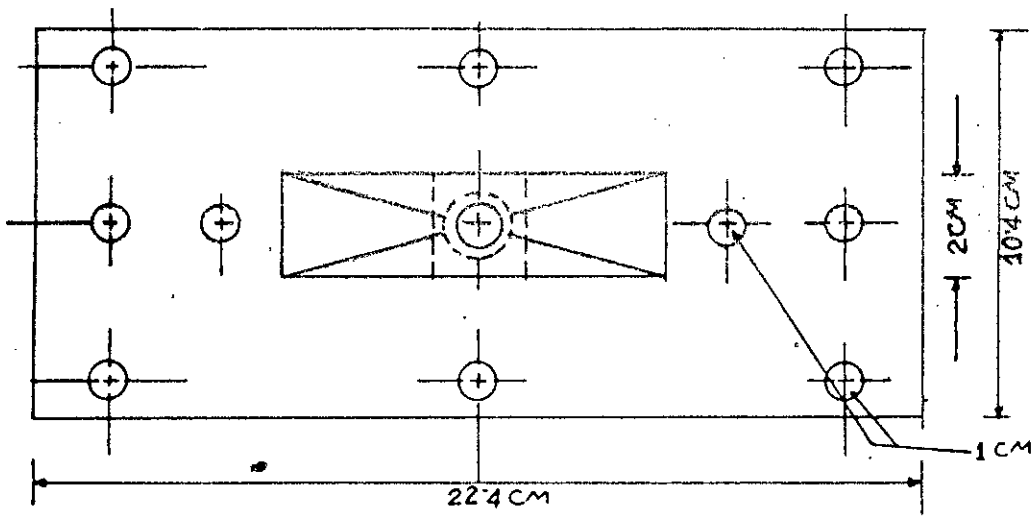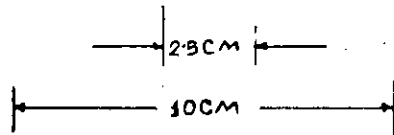
TOP VIEW

FIGURE: 3.1 THE INLET SECTION
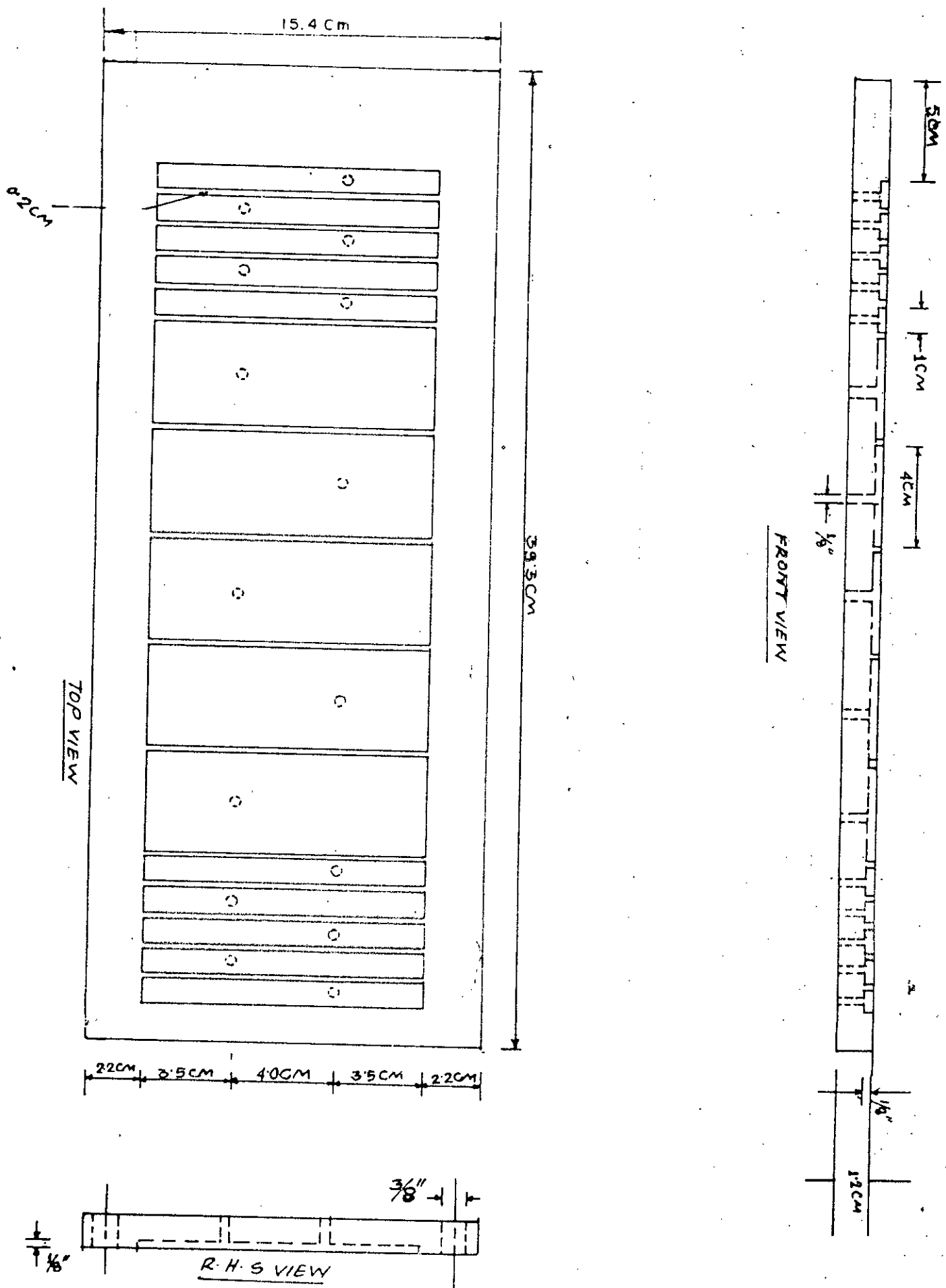
FIGURE: 3.2 THE CATHODE PLATE

R.H.S VIEW

FRONT VIEW
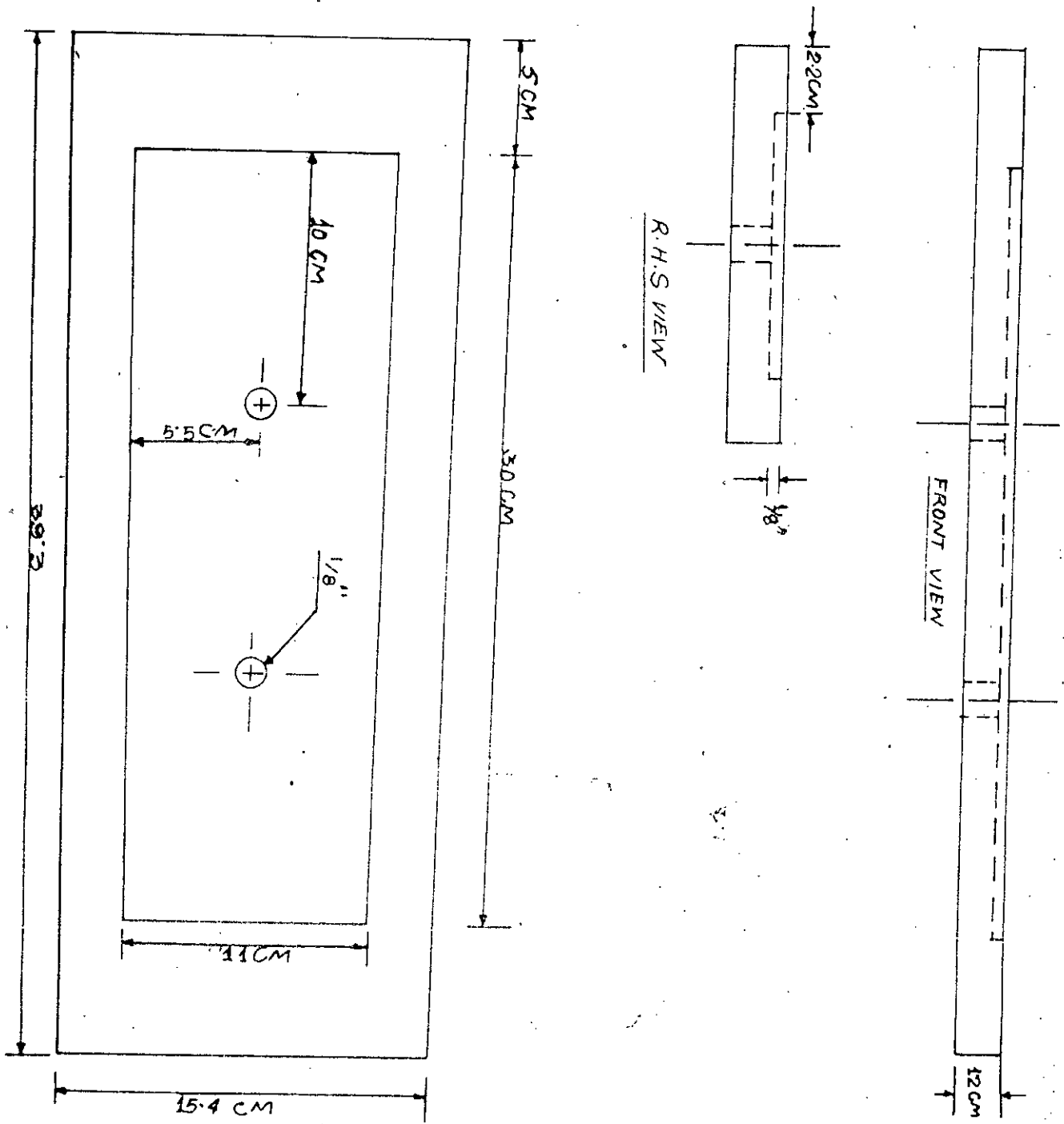
FIGURE: 3.3 THE ANODE PLATE
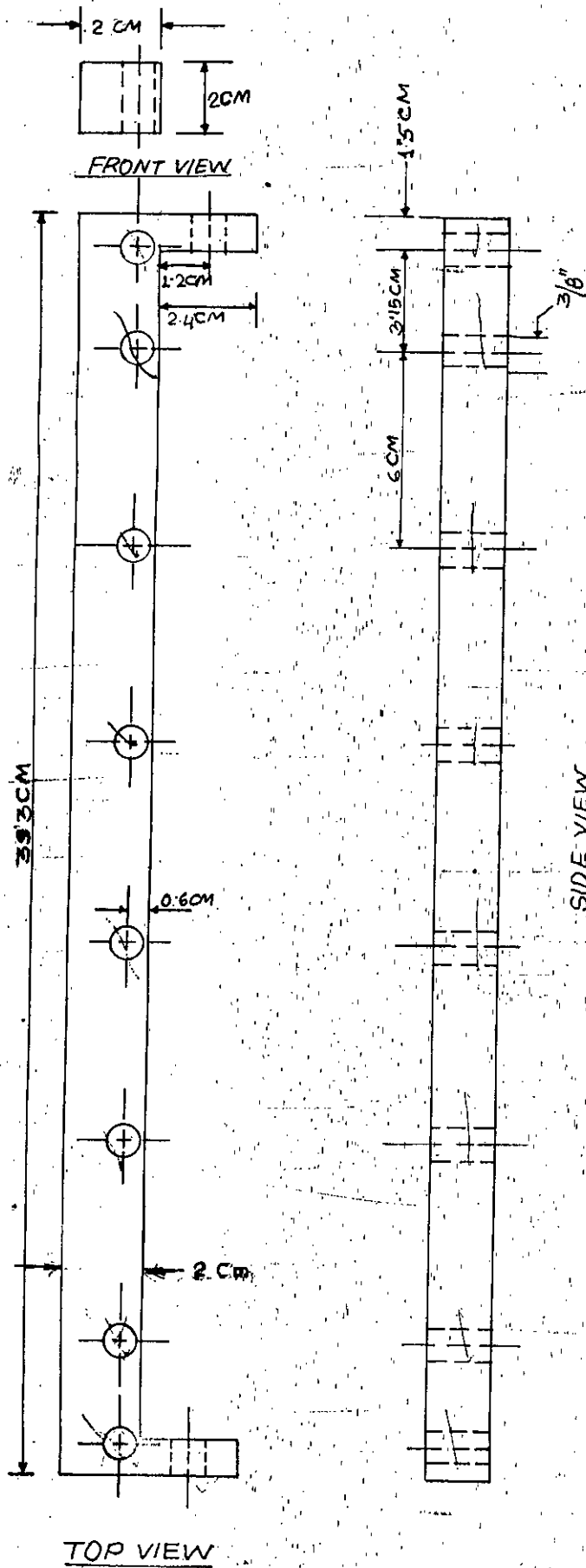
FIGURE: 3.4 THE SIDE PLATE
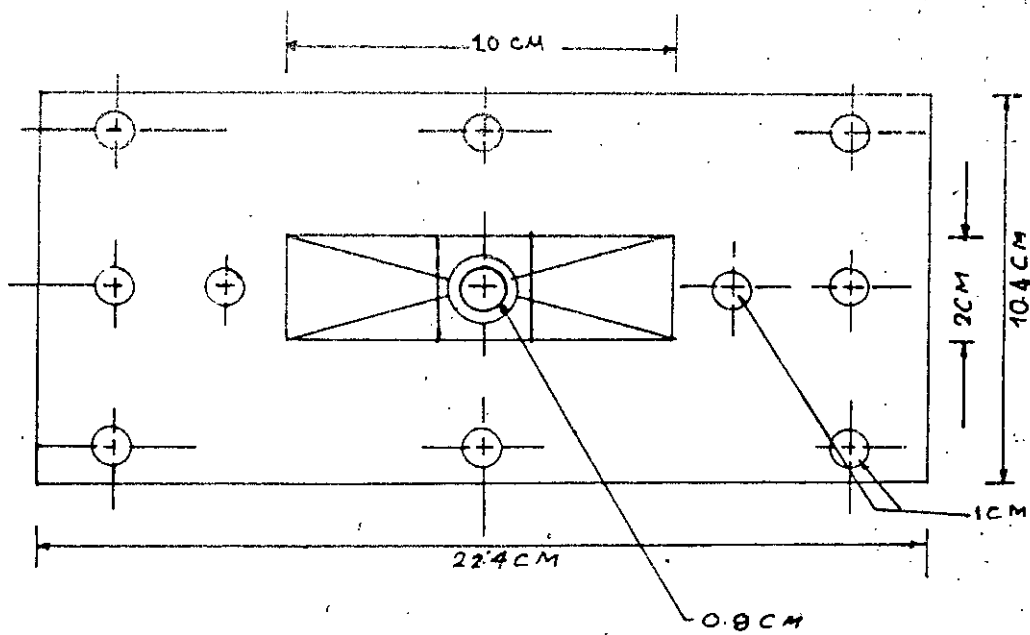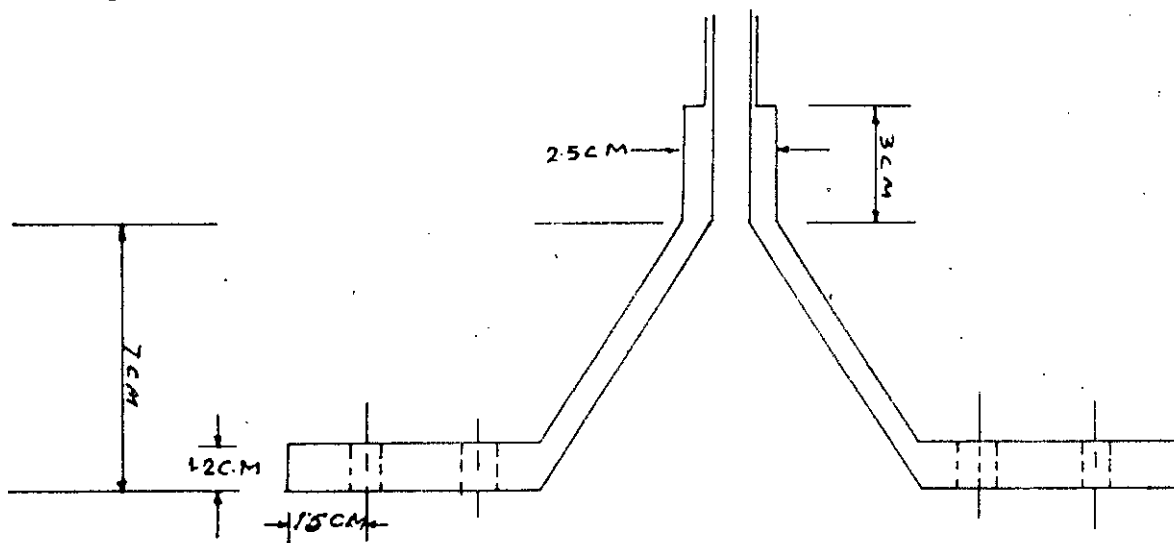
FIGURE: 3.5 THE EXIT SECTION

sufficiently similar to air to render it an acceptable
substitute.

3.2   MAIN EXPERIMENTAL SYSTEM

3.2.1   THE ELECTROLYTIC CELL

The cell used in this investigation is simple in
construction with five sections, the inlet (diffuser with
gas sparger), the cathode side, the anode side, the side
plates, the exit section (reducer). The inlet and outlet
sections were provided to connect the cell to 1/2" PVC
tubing. All the five parts are detachable with the
exception that the side plates are parmanently attached
to the anode side. The electrolyte and gas entered at the
bottom of the cell and flowed upward. There was no
entrance length so that the hydrodynamic and mass
transfer boundary layer started at the leading edge of
the electrode. Figures 3.1, 3.2, 3.3, 3.4 and 3.5 shows
the five main parts of the cell with detailed dimensions.

The cell was constructed out of perspex, the main body
of the cell measuring 39.3 cm X 15.4 cm X 4.4 cm with
anode and cathode plates, each having dimensions of
39.3cm X 15.4cm X 1.2cm, kept at a distance of 2 cm from
one another by two side plates (39.3cm X 2cm X 1.2cm),
these providing a total available cross-sectional flow

area of 10 cm X 2cm ($=20$ cm^2). The anode was a piece of 1/8" thick copper plate (30cm X 11 cm) cemented into the perspex wall with araldite and since the side perspex plates were fitted along the long edges, the exposed anode was 30 cm X 10 cm (= 300 cm^2 area). The electrical connections were made with two 1/16" diameter copper wires soldered to the back of the anode through two 3/8" holes drilled at two positions.

The cathode was 30 cm long and 11 cm wide, but the width of the electrode exposed in the cell was 10 cm due to side plates as it was with the anode. The cathode was divided into fifteen sections from the leading edge of the electrode, the lengths of the section being : 1.0, 1.0,1.0,1.0,1.0,4.0,4.0,4.0,4.0,4.0,1.0,1.0,1.0,1.0 and 1.0 cms, and this is shown in figure 3.3. The cathode sections were arranged in this order as it was anticipated that the mass transfer rates would vary greatly at the inlet and exit regions of the cathode, depending on flow conditions and the shape of the entrance and exit regions. Small sections in these regions enabled more accurate measurements of the variations in current distribution. Each cathode section was fixed with Araldite to a groove of corresponding size cut into the perspex sheet and separated from the adjacent electrode by thin strip of perspex material of

36

0.2 cm thickness. This facilitated the measurement of the current in each section without interference from the neighbouring sections. The electrical connections to each cathodic section were made with fifteen 1/16" diameter copper wires soldered to the back of each cathode segment through fifteen 1/8" holes drilled from the back.

The anode and side plates were fixed together with help of ethylene dichlorine solvent (To hold the cathode and anode plates in their proper position six small steel tubes were used in six location holes) Two rubber gaskets measuring 39.3 cmX2.4 cm made from a bicycle tyre tube and attached with Araldite to the exposed faces of the side plates were used to prevent leakage from the sides of the cell, but this did not work very efficiently and seepage of electrolyte from the sides was a constant problem especially at higher electrolyte flow rates and with simultaneous liquid and gas flows similar leakage problem also occurred at the reducer and diffuser mating faces with the cell body. The main cell body, the inlet and outlet were tightened together with 1/4" diameter brass tie rods through six 1/4" holes bored in the entry and exit section flanges.

The diffuser and reducer were of the same dimensions with the exception of the gas sparger attached to the
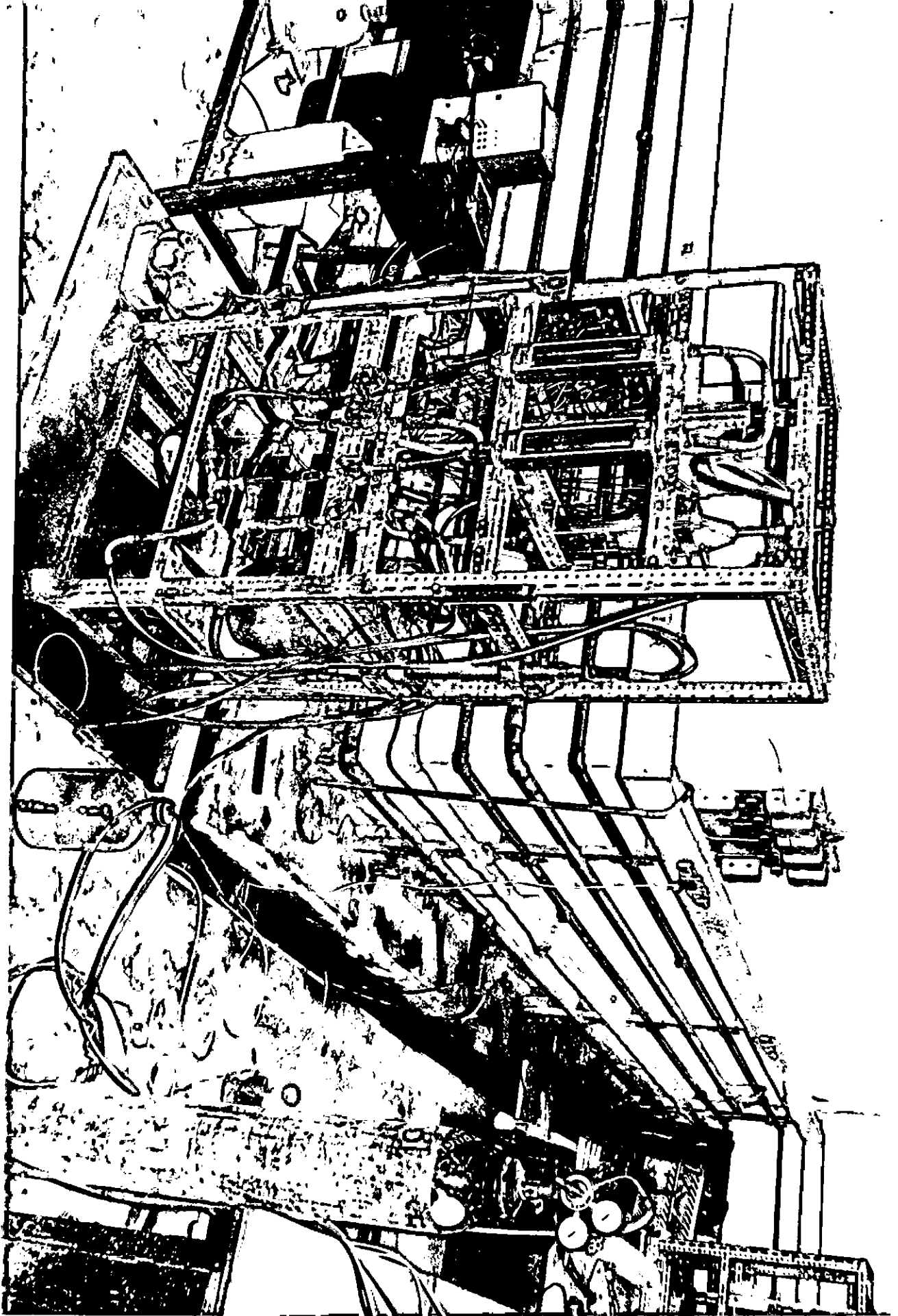
FIGURE 3.6   THE EXPERIMENTAL SET-UP

diffuser. The inside diameters of the portion of the diffuser and reducer at the connection point to 1/2" tubing were 0.8 cm and the flow area (rectangular cross section) increased to 20 cm^2 at the connection point with the cell body. The flanges of the reducer and diffuser were extended (22.4 cm X 10.4 cm X 1.2 cm) to provide sufficient space for tie-rods. The gas sparger connected to the diffuser was 15 cm long, 1.0 cm outside diameter with 19 holes (1 mm diameter) on a pitch of 5 mm.

3.2.2   THE FLOW SYSTEM

The whole flow system was consisted of a pump, a heat exchanger (cooler), three rotameters (one for gas flow measurement), the electrochemical cell, a storage tank and seven two way glass valves. Except the pump, the entire system was mounted on a "Dexion" framework as shown in figure 3.6 which also shows the electrical connections to the cell and electrical measuring devices together with the gas flow system. Figure 3-7 is a more simplified diagram of the flow circuit of the system.

An Electronidioren werke-kaiser pump (with a rating of 220V, 2.15A, 0.25 KW and 60 Hz) with corrosion resistant plastic impeller and fittings was used to circulate the acidified copper sulphate solution from a 20 litre capacity plastic tank through the whole system. The
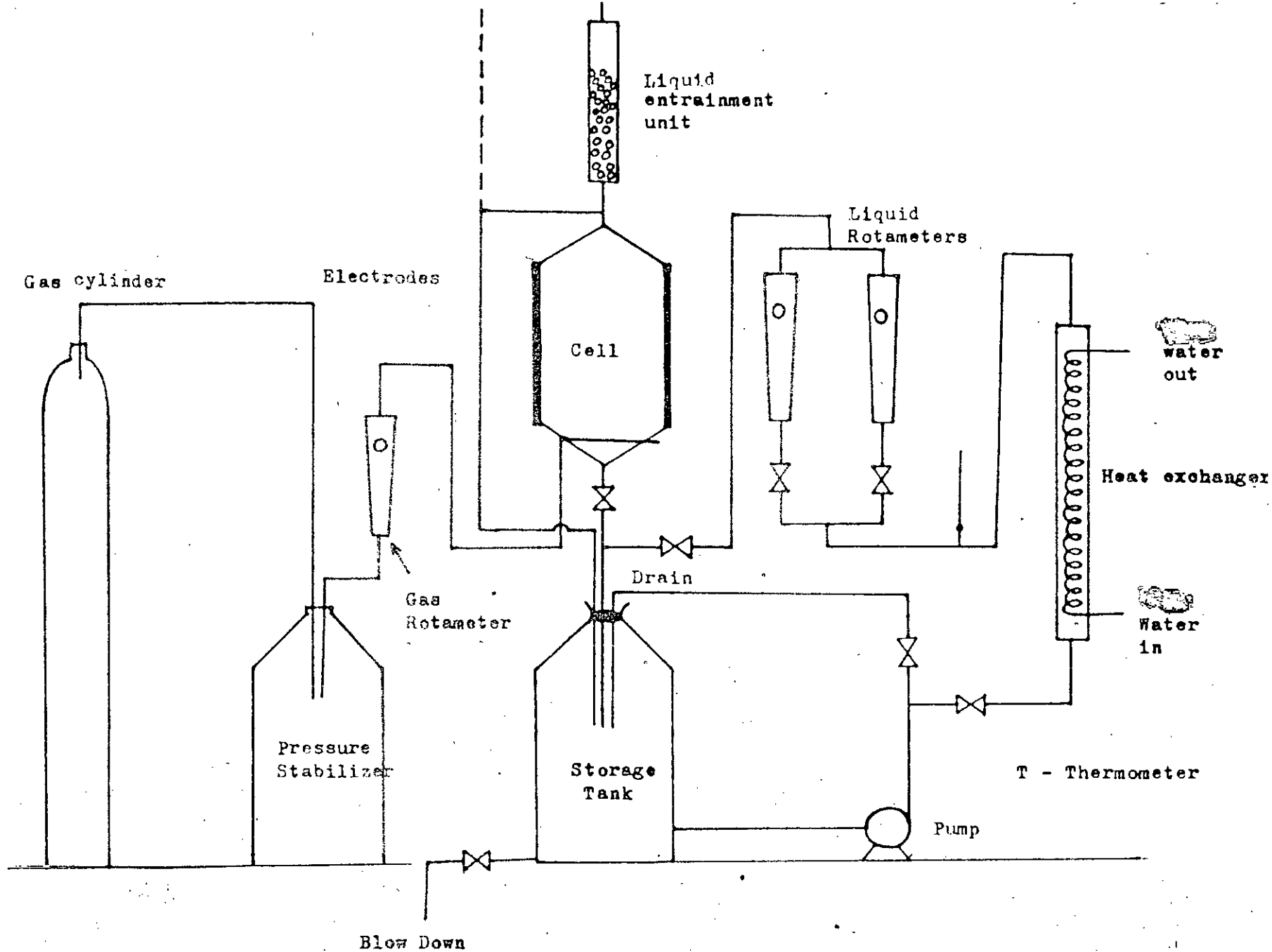
Figure 3.7. Flow circuit diagram.

fittings used was 1/2" PVC tubing and the electrolyte flow rates were measured with the help of a rotameter.

The calibration curve for the rotameter for 0.015 M copper sulphate in 1.5 M sulphuric acid at the temperature of operation has been presented in Appendix B. The flow through the cell could be accurately adjusted by using the flow bypass and three two-way pyrex 1/2" glass valves upstream from the Rotameter. The flow direction in the cell was always vertically upwards.

Since the temperature difference across the cell was small, only one thermometer was used to record the temperature at the inlet of the reactor. The main heating effect in the flow circuit was due to head losses in the circuit producing heat and the temperature of the electrolyte was kept constant at about 30°C by passing cold tap water in a glass heat exchanger mounted in the flow circuit. The thermometer was immersed in the system by means of a glass tee.

The gas sparger connected to the diffuser at the bottom of the cell enabled oxygen free nitrogen from a gas cylinder to be used to deoxygenate the electrolyte. Its main use, of course was to inject gas at different flow rates through stationary electrolyte and with

simultaneous electrolyte recirculation when performing the experiments: A Rotameter was used to measure gas flow rate which was calibrated using soap-bubble method. A pressure stabilizer unit was also connected to the system to keep the gas pressure constant at the orifices to ensure steady flow of gas through the stationary and flowing electrolyte in the cell.

A liquid seperation unit, 2/3 of its length filled with glass rings, was mounted from the cell to the aspirator bottle due to the flow of gas. The glass rings allowed the gas to pass but entrained the liquid and the unit also maintained a height sufficient to prevent the solution going to the aspirator. Two two-way control valves connected through a tee was used at the bottom of the cell to enable the following electrolyte flow arrangements to be made when necessary. These were (a) to keep the electrolyte stationary in the cell when performing stationary selection experiments,(b) to make the electrolyte flow through the cell during experimental measurements under flow conditions; and (c) to drain the electrolyte from the reactor and the whole system to the storage tank after completion of an experiment.
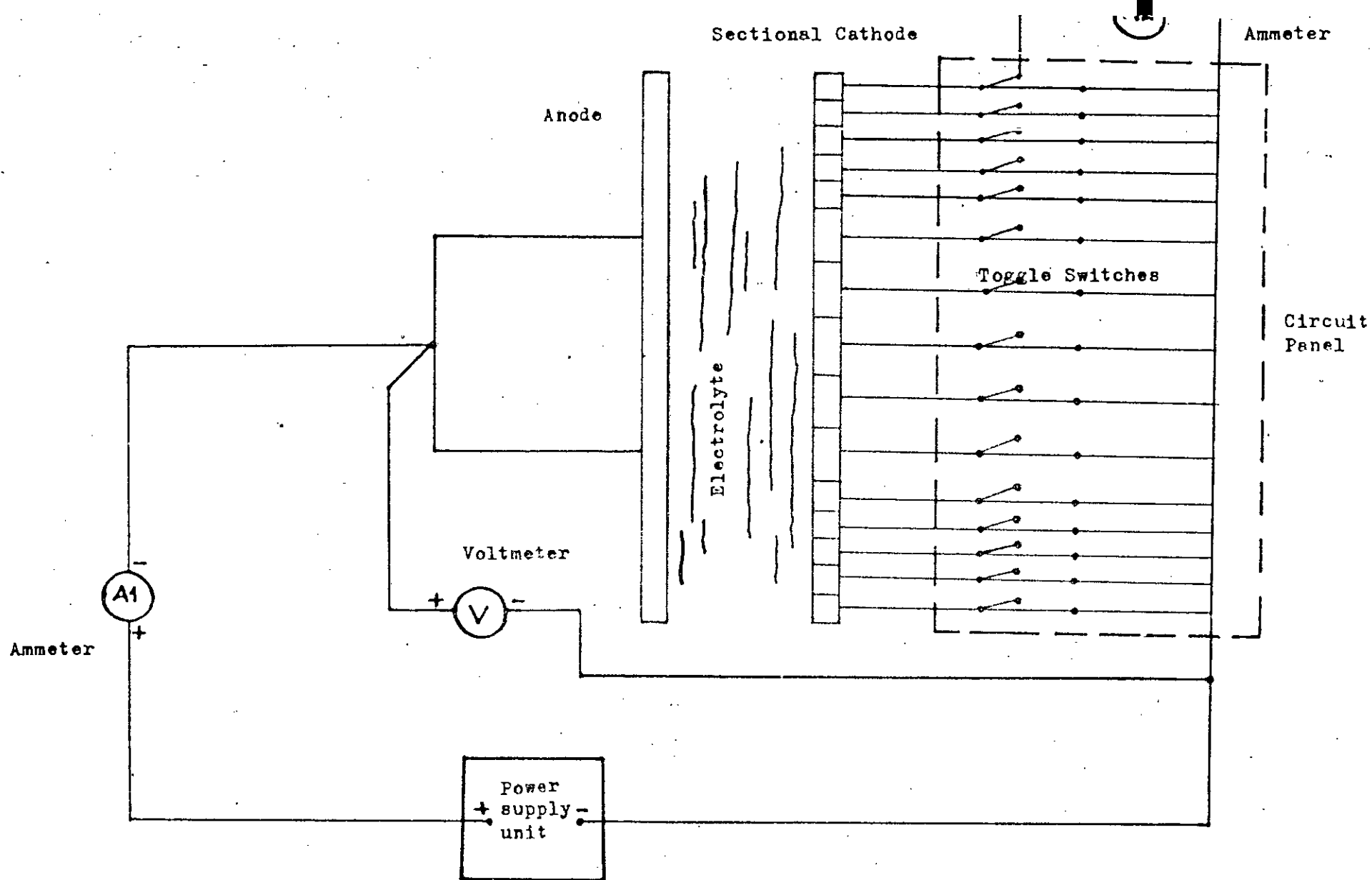
Figure 3.8 Electrical circuit for measuring current at electrode.

3.2.3 THE ELECTRICAL CIRCUIT

An electrical circuit was designed for the electrochemical reactor which would allow the measurement of current on each section of the cathode seperately without interfering with the main electrolytic process or changing the total current passing through the electrode. The electrical circuit is shown in figure 3.8 and a general view of the cell and the delectrical equipment used are shown in 3.6.

An INCO d.c. power supply type 1ZS-5/71-(polish origin) connected to the domestic 220 V line for its energy source, was used which gave a maximum of 500 V and 3.15 A. The total cell voltage was measured by a Sanwa YX-360TR type multimeter placed across the cell. The total current passing through the cell was noted with the help of three different model 301 d.c. ammeters (A1) of Weston Electrical Instruments company having ranges (0-1)A, (0-3)A and (0-15) A respectively and they were of reasonable accuracy. The individual sectioned currents were measured with WESTON type D.C. Ammeter (A2) with a range of 0 to 1 ampere. Toggle switches were utilized to switch away from the main circuit to any section of the cathode, the current being diverted through the second ammeter to give a reading for current on that section and cathode current in all the sections were measured in turn.

41

3.2.4   **EXPERIMENTAL   PROCEDURE**

The concentration of copper sulphate solutions used in the experiments were approximately 0.015M in 1.5M sulphuric acid. Twenty litres of electrolyte solutions were made with analytical grade copper sulphate pentahydrate crystals ($CuSO_4$, $5H_2O$) by dissolving in distilled water. The solution concentrations were determined volumetrically. The method used for the method used for the computation of the concentration of copper sulphate is outlined in Jabbar et el (1972) and Vogel (1961) involving the precipitation of copper as cuprous iodide with excess potassium iodide and titration of iodine formed with standard sodium thiosulphate solution. Analysis of the copper sulphate content was done after a series of runs. Dilute solutions of copper sulphate were used to ensure small limiting currents with correspondingly low rates of dissolution of the anode and deposition on the cathode and minimum natural convection.

Since the activation overpotential of an electrode is greatly dependent on electrode surface, both the electrodes were cleaned before assembling the cell prior to each run. This was done by rubbing the electrode surface with successively finer grades of 'sand' paper and eventually finishing with ultra fine number '0' grade ' 'emery' paper. The electrodes were then rinsed

42

with distilled water, degreased with an organic solvent acetone and the procedure was repeated several times until the electrode surface was properly cleaned. The cleaned electrode surface was finally washed with distilled water and left to dry in air.

The electrical connections to each cathode sections and anode were cleaned and then tested with a multimeter and the conductance between neighbouring sections was also tested in order to make sure that there was no electrical short circuits between the sections of the cathode. Since perspex, the insulator between two sections of cathode, did not react at all with acid solutions, the connection between sections can occur only due to copper deposition. When such a case arose, the deposit between the respective sections were rubbed off with 'sand' paper. If the electrical circuits were found to be satisfactory, the cell was assembled, connected to the flow system as shown in Figures 3.6 and 3.8, sealed with araldite and left for about twenty four hours for setting of the resin.

On startup of the pump, the elctrolyte was recirculated through the system with flow rate adjusted by means of the valves and metered by the rotameter as shown in Fig. 3.9. To expel air from the flow circuit the cell was

43

filled up slowly and then electrolyte was put through the cell at maximum rate to remove air bubbles from the system.

To investigate the limiting current at a given flow rate the applied voltage was set at a definite value by means of the power source and two to three minutes was allowed for the system to reach steady state before the current readings were taken. The individual sectioned currents on the cathode and the total cell currents were measured on the two ammeters. The applied voltage was then increased in steps with intervals of 100 mV and the potential was increased until the individual currents on the sections had exceeded their limiting values. This is signified by the start of the secondary reaction, hydrogen gas evolution at the cathode and a sharp increase in current. After completion of each set of readings the cell was emptied and the power source turned off and at the end of each run the cell was dismantled.

The electrolyte was pumped from the aspirator bottle to the cell until the cell was filled with electrolyte and nitrogen was sparged from the gas sparger for about one hour to deoxygenate the solution. The liquid seperation unit was mounted at the top of the cell to prevent the overflow of the electrolyte to the storage tank during

experiment using gas sparging through stationary electrolyte. For simultaneous gas-liquid flow this seperation unit has been cut off. The pressure stabilizer unit ensured the steady supply of gas through the electrolyte and a mesh distributor with a layer of glass beads of 2-3 mm in diameter about 2 cm high at the top of the gas sparger was provided to keep the bubble size uniform. To get an even deposit the cell was first operated at low current densities of 0.2 mA/cm^2 to 0.3 mA/cm^2 at the required flow rate for about 15-20 minutes.

3.2.5   **MEASUREMENTS   OF   BUBBLE   SIZE DISTRIBUTIONS**

The bubble size distribution was photographed in a rectangular duct measuring 39.3cmX15.4cmX2cm, made of 1/4" transparent perspex sheet and joined together with perspex cement and araldite. This replaced the electrolytic cell which was used in the measurement of current-voltage of the system, but it is as the same size as the cell. This was done because bubbles could not be seen from outside in the electrolytic cell. The photographs were enlarged to enable the size range to be analysed and the bubble size was determined manually without any size analyzer.

An area was chosen where a sizeable number of bubbles were present. The bubbles were of different shapes, mostly spherical, some of them are approximately spherical and a few of them were elliptical and in between. The actual bubble size was determined from the photographic bubble size divided by ratio of magnification factor of photographic area to the actual area. The table of photographic bubble size distribution has been presented in Appendix.

CHAPTER   4

RESULTS AND DISCUSSIONS

4.1.   INTRODUCTION

In the electrolysis of copper sulphate-sulphuric acid solution, the rate of copper deposition at the cathode is controlled by the rate of mass transfer across a diffusion layer. The cathode was sectioned to enable the measurement of the variation of current density distribution and hence the rate of mass transfer along its length. In the present study, dilute solutions of acidified copper sulphate (0.015 M) have been used as the electrolyte in order to keep the value of limiting current low. In all the runs, individual current on the sections of the cathode and the total current were measured at different applied voltages specially at the limiting current conditions.

Experimental work was carried out in order to study the influence of the following modes of forced convection on the mass transfer rate on the deposition at the cathode in the electrochemical reactor:

1.   Sparging of gas bubbles through stationary solutions.

2. Forced circulation of electrolyte with simultaneous sparging of gas bubbles through the electrolyte.

The flow rate of gas in the system varied between 1.65 lit/min to 14.65 lit/min, the latter being the maximum flow rate that could be measured by the available gas rotameter. The maximum flow rate of electrolyte was limited to 7.8 lit/min so that no leakage occurs in the cell due to high pressure on the cell surface and the electrolyte was kept at temperature $(30 \pm 2)^{\circ}$ C.

4.2. **PRESENTATION AND ANALYSIS OF RESULTS**

The individual current on the sections of the cathode and the total current were measured at different flow rates by increasing the applied voltages in steps until all the sectioned elements attained and exceeded their limiting current conditions. The reproducibility of the data collected was checked by making repeated runs which showed reasonably good agreement of around ± 5% .

The total current and the current passing through different sections of the electrode have been computed. The summation of the current of different sections at limiting condition was within 3% of the total measured current. The experimental data and calculated results

were presented in Appendix C for gas sparging through stationary electrolyte and in Appendix D for simultaneous gas-liquid flow.

Since the current measurement at an electrode section is not a point value but covers the entire area of the electrode section element, it is most useful to represent the variation of the percentage of the total current flowing at different sections along the length of the electrode in the form of a histogram. A number of such histograms have been shown for different gas flow rates in case of gas sparging and at different set of gas-liquid flow rate in case of simultaneous flow.

From the total current-voltage curve, the overall limiting current can be derived and used to obtain a correlation for the overall mass transfer coefficient (k_g) as a function of flow rate. The average mass transfer coefficient (k_{avg}) over an electrode sections and the variation of the average mass transfer coefficient along the length of the electrode was also calculated by progressively averaging the individual mass transfer coefficients over the length of the electrode. The average mass transfer coefficient was plotted against L/D_e to obtain correlation at different gas flow rate.

Comparison was made with other mass transfer correlation that was obtained either empirically or semitheoretically by other workers.

To obtain useful mass transfer correlation in this system, knowledge of bubble size distribution, the average bubble diameter and the volume fraction of gas present in the solution at different gas flow rates could not be observed or measured in the cell during the experimental work. It was done using a clear perspex rectangular duct having the same dimension as that of the cell to produce the same hydrodynamic condition and approximately the same bubble size distribution at different flow rates as that of the electrolytic cell. Bubble size distribution have been obtained from photographs of air bubbles at different flow rates and average bubble diameters have been calculated on the basis of size distributions.

4.3.1) ANALYSIS OF BUBBLE SIZE DISTRIBUTION

The bubble size distribution is an important parameter when gas injection is used to enhance the mass transfer rate by stirring the electrolyte. When gas is sparged through the orifices (of diameter 1 mm) of the gas sparger, the gas bubbles may be distributed in the

Glass bead

Mesh distributor

Air sparger.
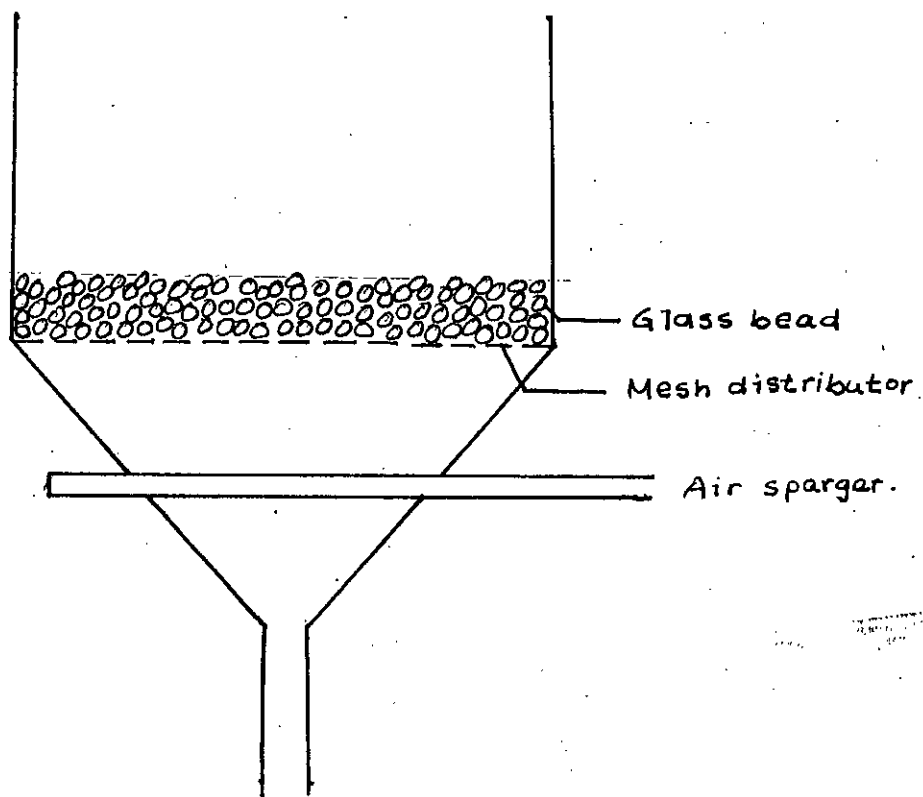
FIGURE 4-1

electrolyte in different ways, either in the form of individual gas bubbles that float up through a layer of liquid, or consisting of an assembly of bubbles of unequal size due to non-uniform flow through the orifices. However at any point in the dispersion system, the distribution of sizes changes due to both bubble size and variation of velocity. It also may be due to break up of the bubbles by liquid turbulence and coalescence of colliding bubbles along the length of the electrode.

The mechanism of bubble break up, coalescence and size distribution is very complex. Experimental studies were carried out to determine the size distribution and care has been taken to keep the bubble size uniform by putting another mesh distributer with a layer of glass beads (2-3 mm diameter) about 2 cm high at the top of the gas sparger. The arrangement is shown in Figure 4.1.

Gas liquid distributions were photographed to determine the bubble sizes and the analysis of size distribution on a particular differential area chosen over sections of the reactor has been regarded as a representation of the bubble distribution in the overall system. The shape of the majority of the bubbles in the dispersion system can be defined as roughly spherical, although the shapes of the bubbles , specially the larger ones , are of

PLATE 4-1 : GAS FLOW RATE = 8.20 lit/min.
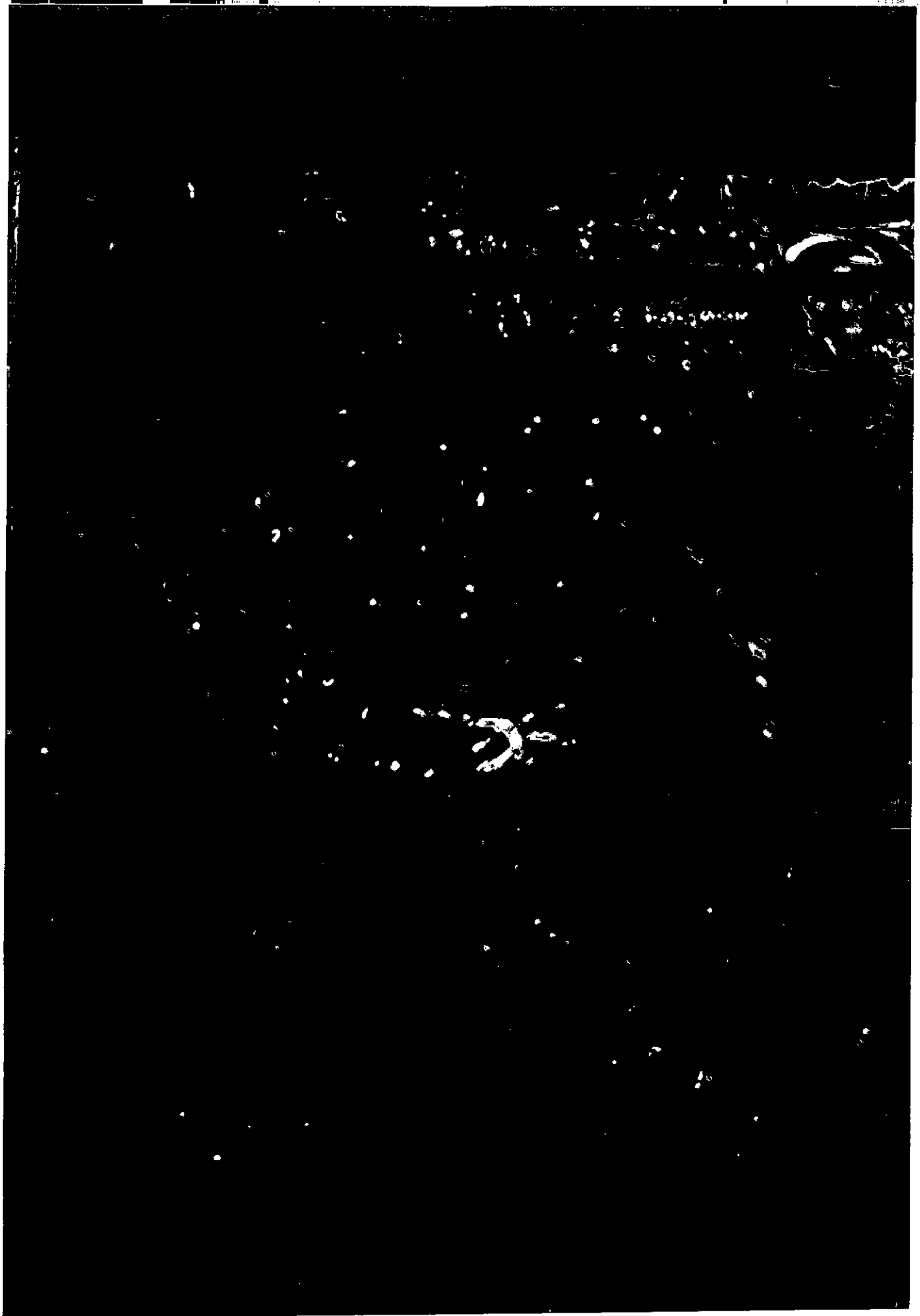
PLATE 4-2: GAS FLOW RATE = 14.65 lit/min.

various shapes. Very small bubbles whose diameters are less than 0.0025 m have been excluded from the experimental data because their contribution to mass transfer rates as well as to the total gas volume and average diameter of the bubble are small.

From the photographs as shown in Plates 4-1 to 4-4, the smaller bubbles are found every where, specially at the edge of the reactor with large size bubbles relatively confined to the central core on the width of the reactor which are due to the uneven distribution of bubbles through some orifices and coalescence of several small bubbles. From the analysis of the bubble sizes from the photograph, the bubbles were arranged in order of their diameters and the series.

4.3.2 ESTIMATION OF AVERAGE BUBBLE DIAMETER

The average bubble diameter is a useful quantity because it enables a Reynolds number and Sherwood number to be defined for the system. However it cannot be determined from any theoretical prediction. Average bubble diameters can be calculated from the bubble size ranges of experimental data and these can be expressed as:

Mean diameter   d = $\Sigma nd/\Sigma n$ ....(4.1)

Log average diameter d_n = exp{$\Sigma n \ln d/\Sigma n$}   (4.2)

Volume to surface mean diameter $d_{vs}=\Sigma nd^3/\Sigma nd^2$ (4.3)

Equation (4.1) cannot be used because it does not
describe the actual system, and equation (4.2) also
cannot be used because the log normal probability
function does not represent the experimental histogram
accurately. Since the volume of the bubbles influences
the mass transfer rate, average bubble diameter on the
basis of volume to surface mean diameter is a reasonable
choice. Table 4.1 shows the average bubble diameter for
different gas flow rates. It has been found that the
bubble diameter decreases with increase in flow rate.

TABLE 4.1   BUBBLE DIAMETER

Gas flow rate	Average bubble diameter volume to surface(mm)	Void fraction
3.25	10.5	–
8.20	9.12	0.1165
14.65	7.97	0.0700

Since no bubble size analyzer has been used, the
calculated diameters are approximate values.
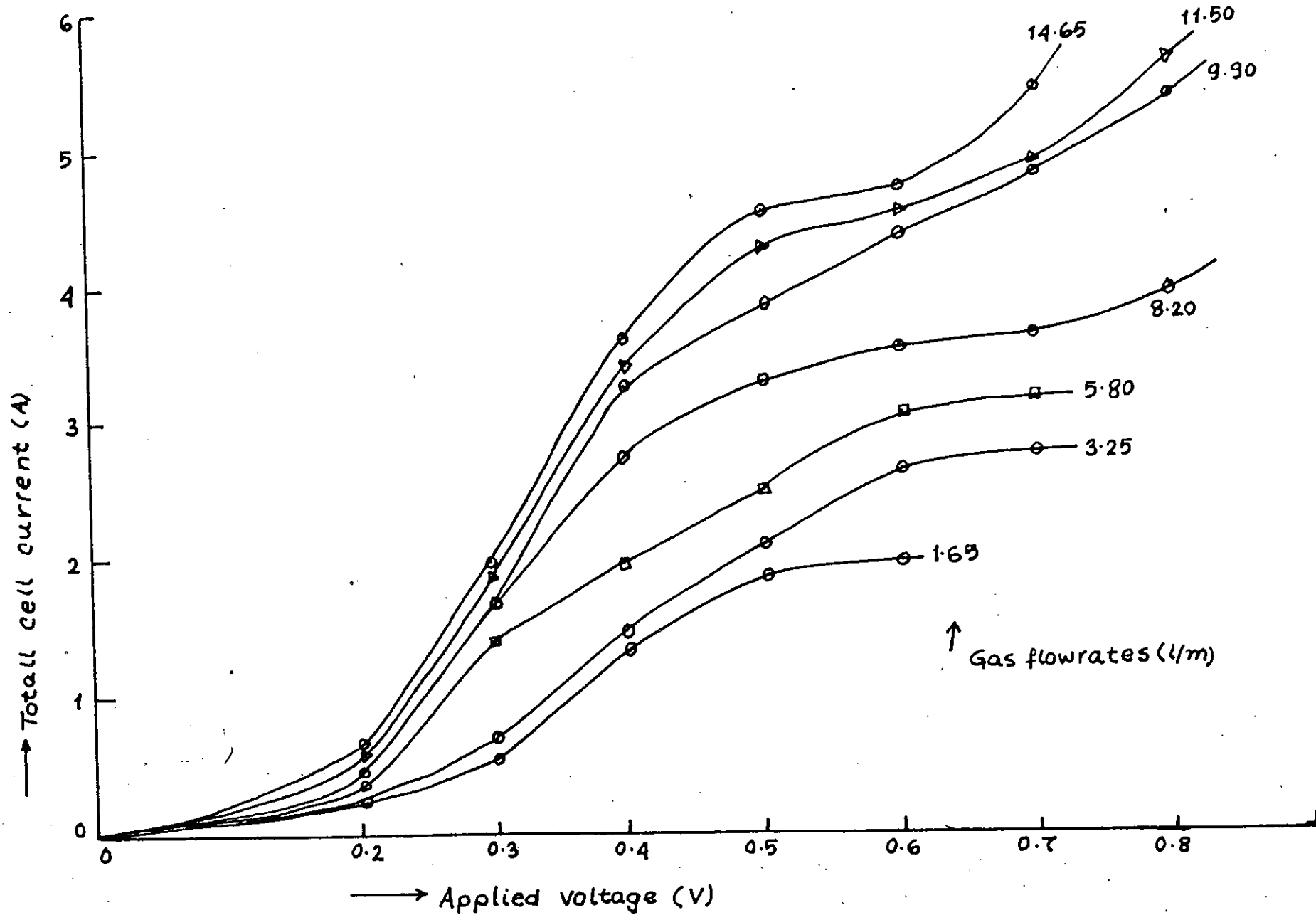
FIGURE 4-3 . CURRENT-VOLTAGE CURVE AT DIFFERENT GAS FLOWRATES

4.4.1. CURRENT—VOLTAGE CURVE FOR GAS SPARGED SYSTEM

The total current and individual current on the sections of the cathode were measured against applied voltages at different gas flow rates and the results were presented in Appendix C. The measured total current was always higher (not more than 3%) than the total current calculated from the summation of the sectional current. This is due to the slight change of circuit impedance when current is being measured accounts for slight differences in two current. The experimental results have been presented in graphical form in Figure 4-3 for seven flow rates from 1.65 lit/min to 14.65 lit/min.

From Figure 4-3 it can be seen that the limiting current plateau is well defined having a potential range of about 100 mV at the lower flow rate of gas, 1.65 lit/min to 5.8 lit/min. The shape of the curve changes as the flow rate is increased and the limiting current regions shows slight rises in current when the gas flow rates were 11.5 lit/min and 14.65 lit/min.
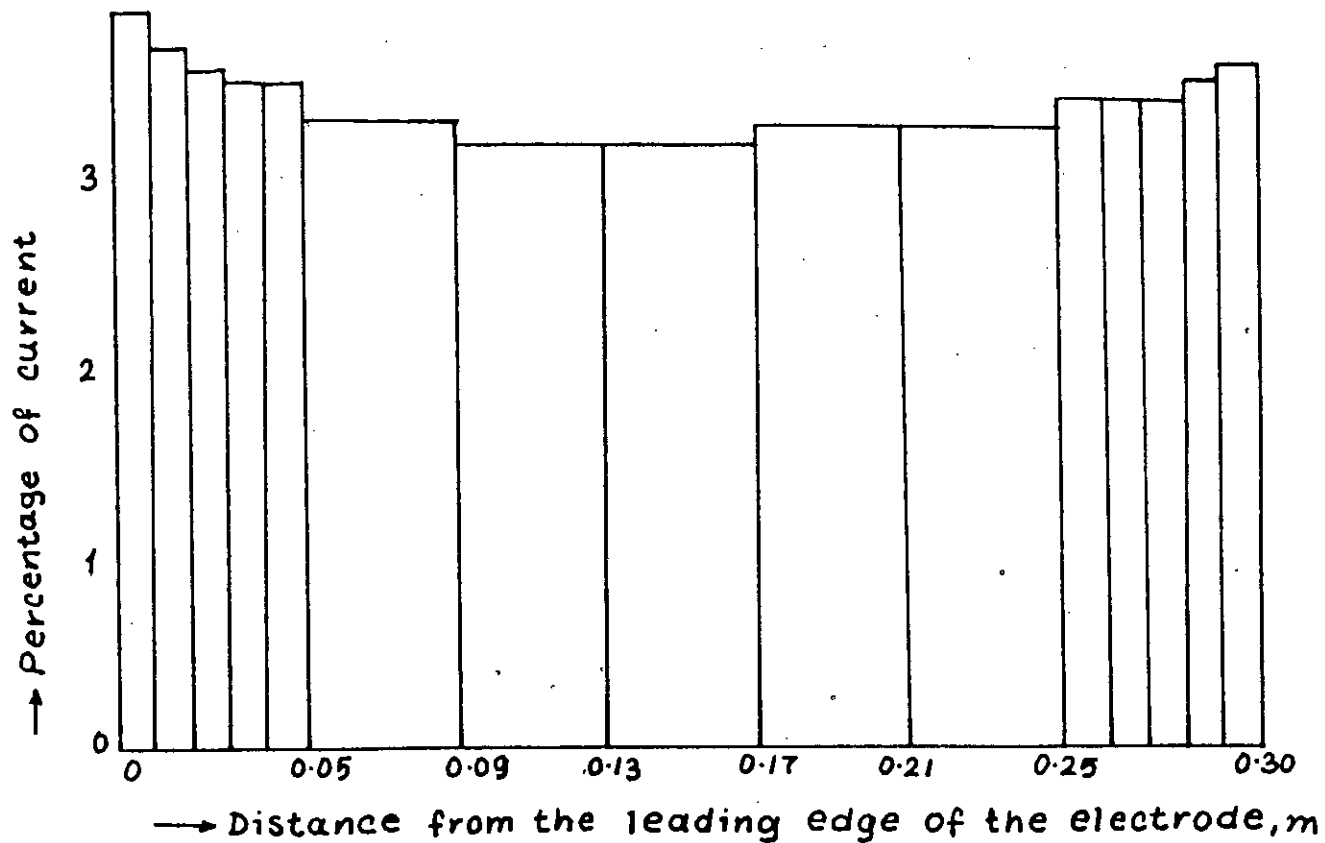
FIGURE 4-4   FRACTION OF CURRENT THROUGH THE SECTIONS
OF THE CATHODE AT GAS FLOWRATE OF 3·25 lit/min.
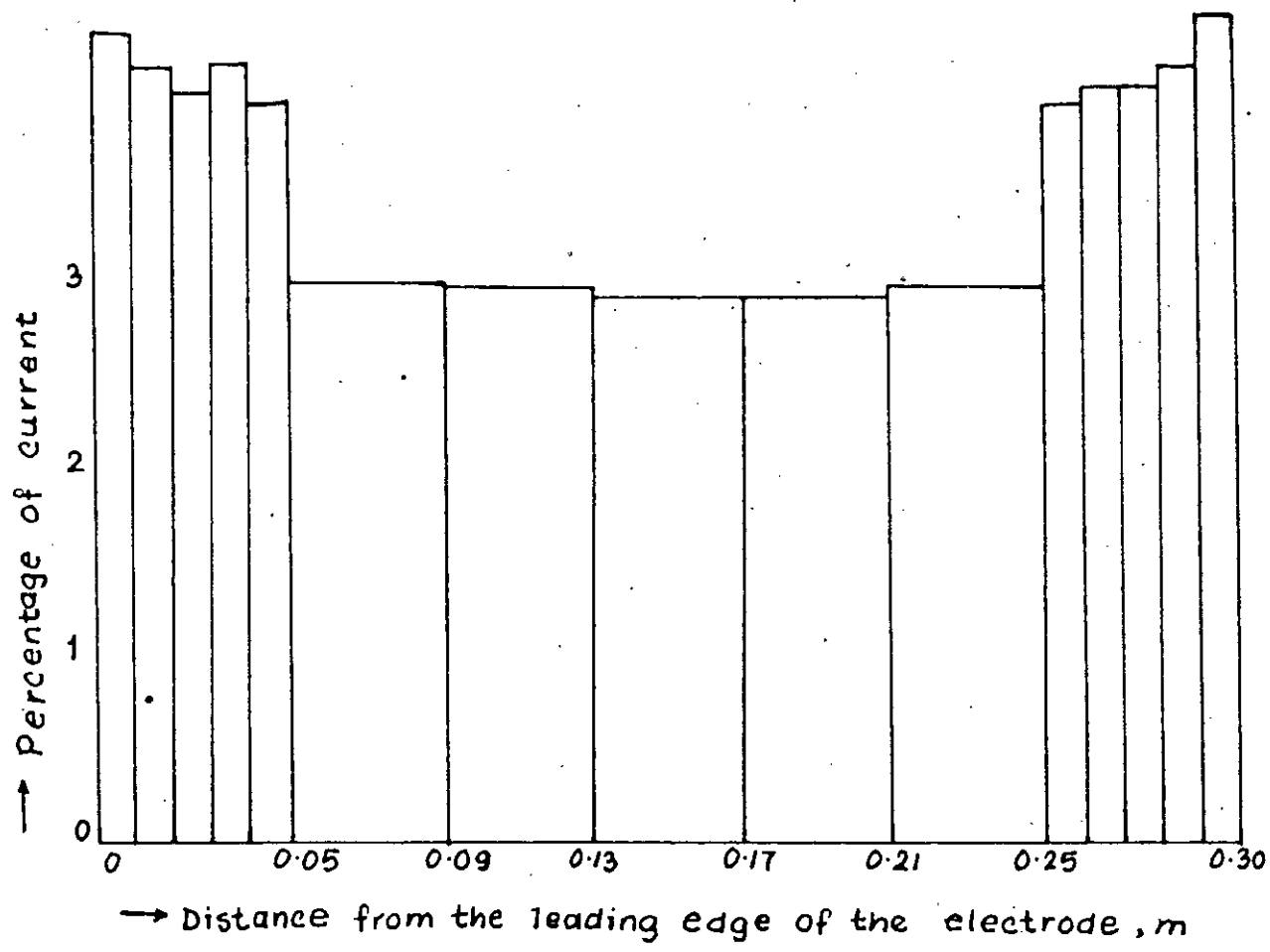
FIGURE 4-5 FRACTION OF CURRENT THROUGH THE SECTIONS

OF THE CATHODE AT GAS FLOWRATE OF 8·20 lit/min.
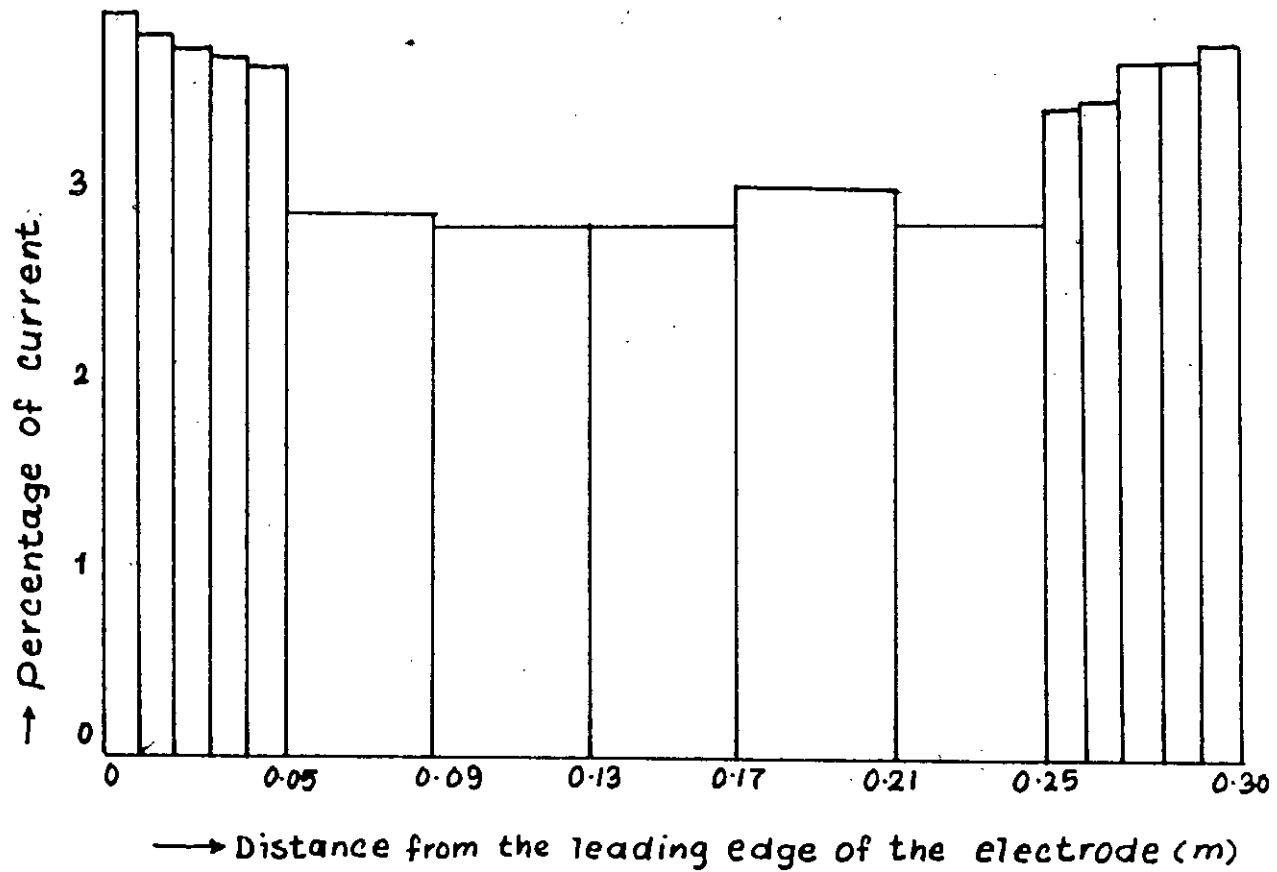
FIGURE 4-6 FRACTION OF CURRENT THROUG⁻ THE SECTIONS

OF THE CATHODE AT GAS FLOWRATE OF 14·65 lit/min.

4.4.2. CURRENT DISTRIBUTION ON THE SECTION OF THE CATHODE

For different gas flow rates , the fraction of current passing through each cathode section has been calculated using the current voltage data. For a given gas flow rate, the fractional current passing through a specific section is approximately constant irrespective of any applied voltage whether the reactor is operating at below or above limiting current condition. For comparison purposes, however, it is useful to compare at limiting current condition because a stable current distribution is reached with the sum of the individual sectional current approximately equal to the total current.

The percentage of current distribution at different gas flow rates at limiting current conditions are shown in Table 4.2 and has been presented in the form of histograms in Figures 4-4, 4-5 and 4-6 for gas flow rates of 3.25, 8.20 and 14.65 lit/min respectively. All these histograms show similar current distributions, there ins an increase in the inlet and exit regions of the cathode due to entrance and exit effects in the reactor. At the entrance region it so happens due to developing velocity and concentration profiles in the boundary layer of the electrolyte. At the exit region such behaviour can be described as the effect of accelerating velocity

55

gradients. Thus turbulence produced by gas flow is more influential at the inlet and exit section of the cathode than at the middle sections.

TABLE 4-2   PERCENTAGE CURRENT DISTRIBUTION AT
                DIFFERENT GAS FLOWRATES

Cathode\ section \	Flow rate (lit/min)	1.65	3.25	5.80	8.20	14.65
1		4.69	3.85	3.92	4.22	3.83
2		4.42	3.66	3.92	4.03	3.72
3		3.87	3.52	3.82	3.90	3.64
4		3.87	3.48	3.85	4.06	3.62
5		3.87	3.48	3.76	3.87	3.57
6		3.52	3.25	2.96	2.94	2.81
7		3.32	3.11	2.87	2.94	2.77
8		3.18	3.11	2.79	2.88	2.77
9		3.81	3.21	2.78	2.88	2.95
10		3.25	3.21	2.81	2.92	2.77
11		3.31	3.37	3.70	3.87	2.36
12		3.87	3.37	3.73	3.95	3.40
13		3.59	3.37	3.85	3.95	3.60
14		3.87	3.48	3.85	4.06	3.60
15		4.14	3.55	3.92	4.31	3.70
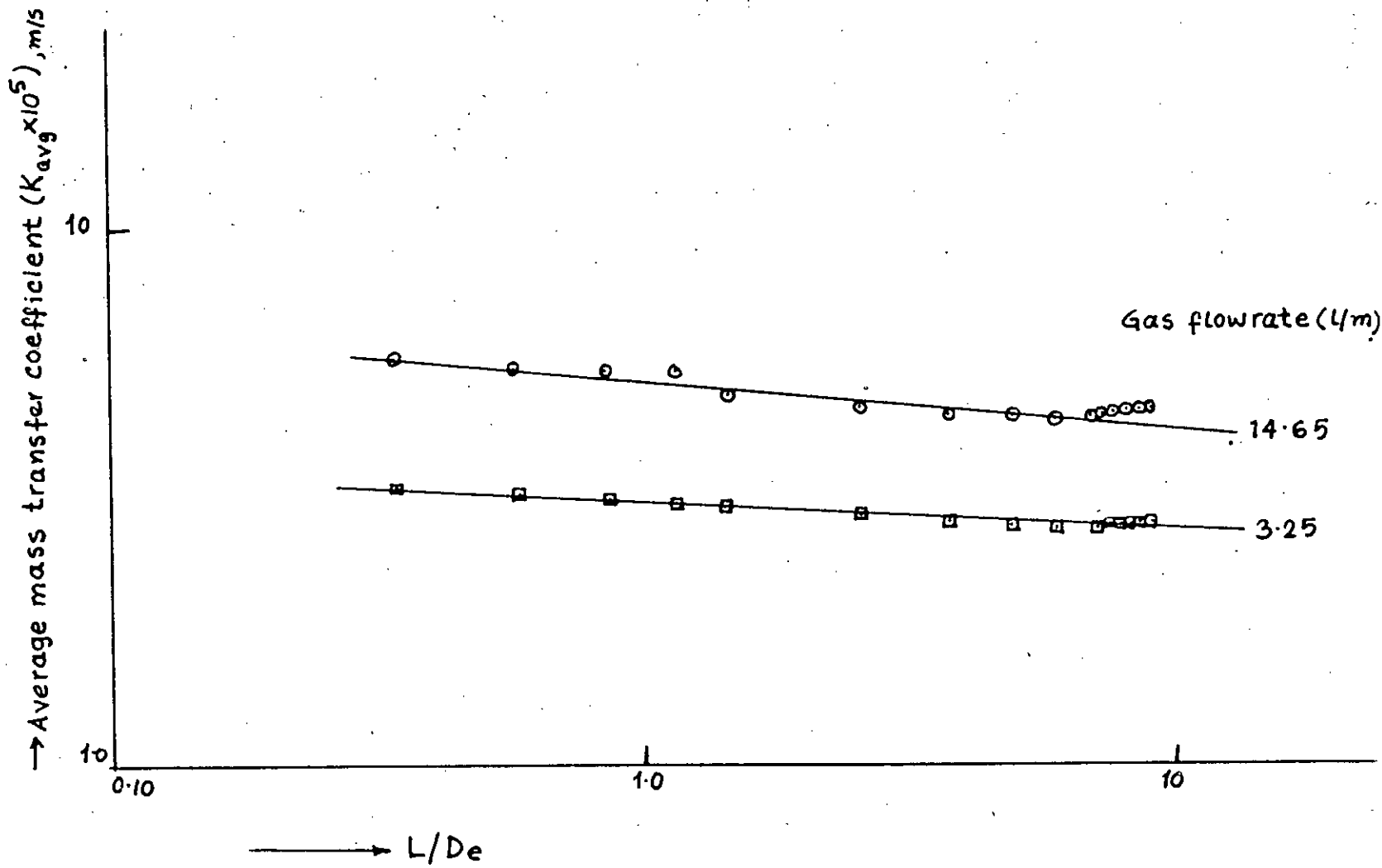
FIGURE 4-7 VARIATION OF AVERAGE MASS TRANSFER COEFFICIENT
ALONG THE LENGTH OF THE ELECTRODE

4.4.3. MASS TRANSFER COEFFICIENT ALONG THE LENGTH OF THE ELECTRODE

Variations in the individual mass transfer coefficients over the cathode sections are, of course, exhibited by the plots of the current distributions along the length of the electrode as shown in Figures 4-4 through 4-6. It shows enhancement of mass transfer at the inlet and exit sections of the cathode in comparison with the middle region (the middle five sections have a total length of 20 cm) of the electrode. This causes as a result of the inlet and exit effects. It reveals that the mass transfer coefficient is approximately independent of distance due to uniform agitation resulting from gas sparging over the electrode. At higher gas flow rates, from 8.20 to 14.65 lit/min, mass transfer rates increase more prominently at the inlet (first five sections) and exit (five sections at the exit) region. This may be due to the formation of large bubbles at the central core in the width of the electrode by the coalescence of several small bubbles. As a result, the air bubbles only stir the electrolyte in some local area in that section and not over the whole region.

Figure 4-7 shows a logarithmic plot of average mass transfer coefficient against L/D_e at two different gas flow rates eg. 3.25 and 14.65 lit/min. The average mass

transfer coefficients have been calculated by progressively averaging the individual mass transfer coefficient on each section and the results have been presented in Appendix C. Although the averaging of the individual mass transfer coefficients is not valid since they are independent of distance. However, it serves as a useful means of comparison and average values have been used. Two theoretical approaches can be made as the Leveque (1928) solution:

$$K_{av} = k_1 (d_e/L)^{1/3} \qquad \ldots\ldots\ldots\ldots(4.4) \quad \text{and}$$

the solution drawn by Ali (1982) as:

$$K_{av} = k_2 (d_e/L)^{0.22} \qquad \ldots\ldots\ldots\ldots(4.5)$$

But neither of them is suitable for interpreting the experimental results in the present system because they have recirculated the electrolyte to enhance the mass transfer rate. Moreover equation (4.4) is applicable for fully developed laminar flow.

In the present study, the curves show a slope of approximately -0.10 , so that mass transfer relationship can be expressed as:

$$Kav \propto (d_e/L)^{0.1} \qquad \ldots\ldots\ldots\ldots(4.6)$$

The value of the exponent 0.10 in equation (4.6) can be compared with that of 0.22 in equation (4.5) because in both the case the mass transfer coefficients are influenced by simultaneously developing hydrodynamic and

58
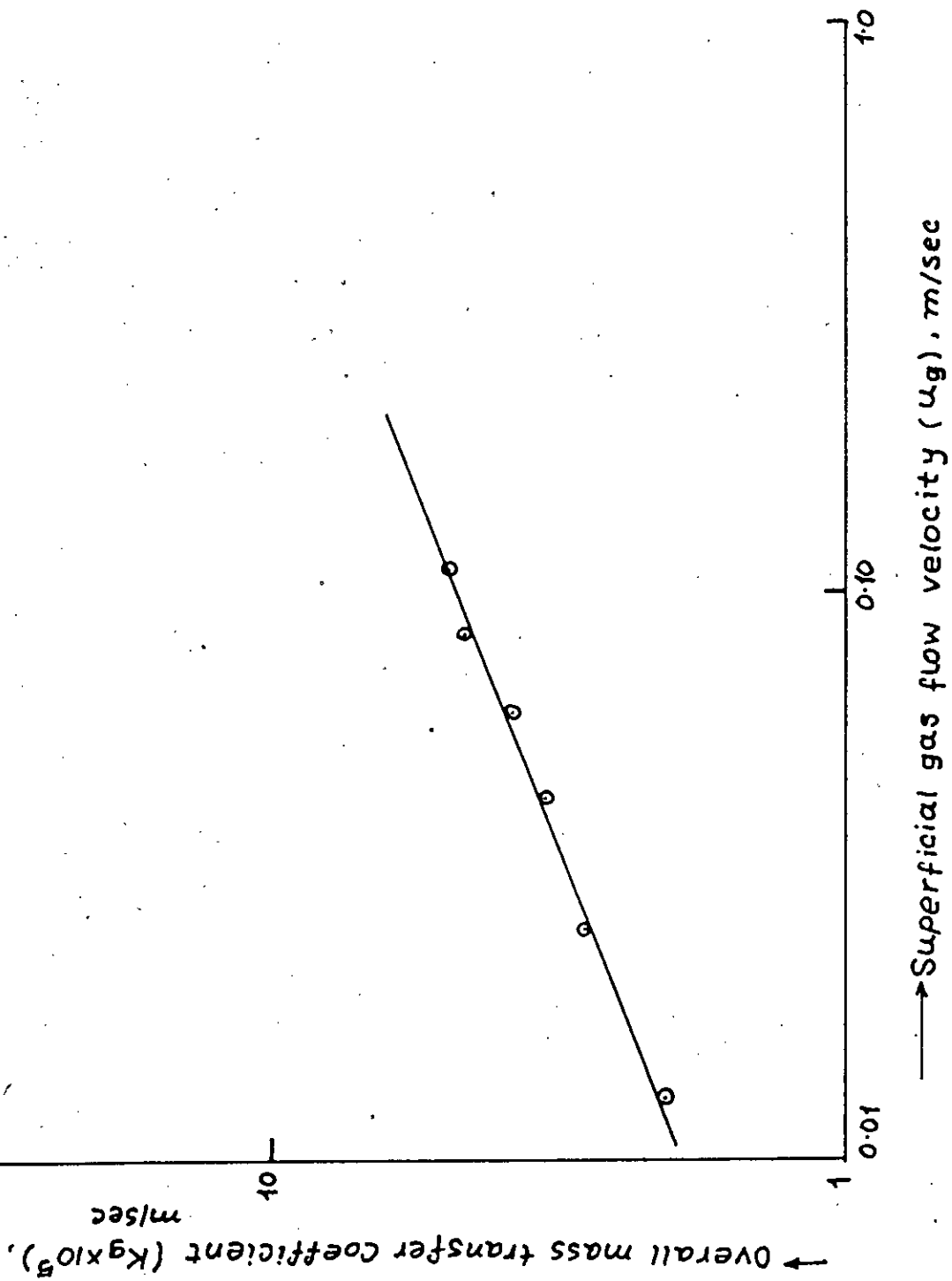
FIGURE 4-8 MASS TRANSFER COEFFICIENT AGAINST SUPERFICIAL GAS VELOCITY

concentration boundary layers as well as the shape of the entrance region.

4.4.4. <u>VARIATION OF MASS TRANSFER COEFFICIENT WITH SUPERFICIAL GAS VELOCITY</u>

The overall mass transfer coefficient calculated from the total measured current at limiting conditions for the entire reactor has been plotted logarithmically against superficial gas velocity as shown in Figure 4.8. Figure 4.8 shows that mass transfer rate increases with superficial gas velocity. The slope of the curve is approximately 0.4 which indicates the exponent of the superficial gas velocity as:

$$K_g \propto u_g^{0.4} \qquad \dots\dots\dots\dots\dots(4.7)$$

The exponent on the superficial velocity is between o.3 and 0.9 which values are for when the bubbles do not coalescence and when the bubbles coalescence easily, respectively.

With the increase in gas flow rate the mass transfer coefficient increases because the intensity of turbulence at the electrode surface is increased. This means that the free stream turbulence of the gas flow , depending on its intensity, will affect the turbulent state of the boundary layer in transverse motion to the electrode
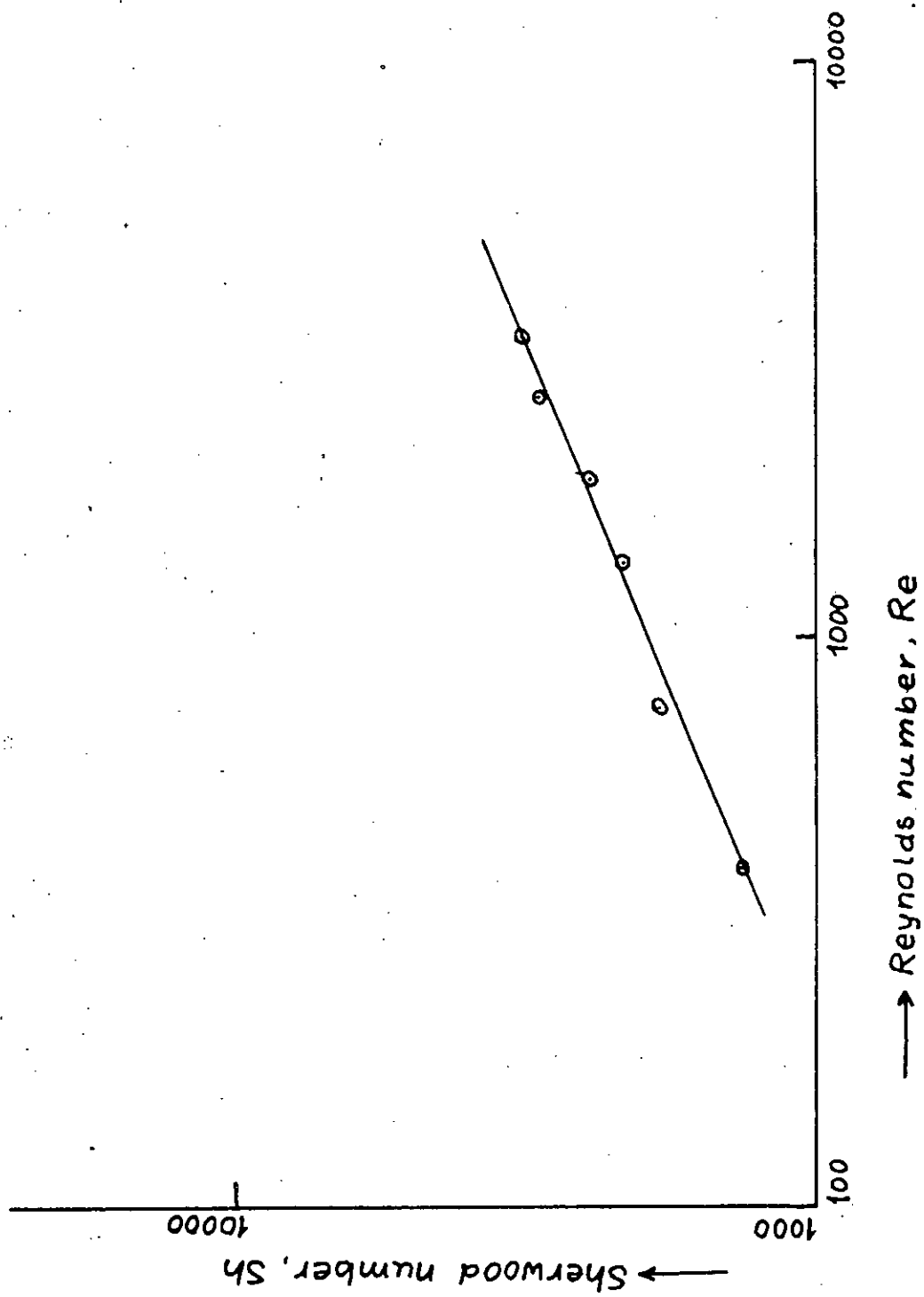
FIGURE 4-9   SHERWOOD NUMBER vs. REYNOLDS NUMBER

surface. Thus the intensity of turbulence at the electrode will increase as the intensity of turbulence of gas sparging increases that is with the increase in gas flow rate. Equation (4.7) can be compared with the study of Ali (1982) who has obtained a correlation as:

$$K_g \propto U_g^{0.6} \quad \ldots\ldots\ldots\ldots\ldots (4.8)$$

4.4.5. OVERALL MASS TRANSFER CORRELATION

An overall mass transfer correlation can be obtained by plotting Sherwood number against Reynolds number calculated using gas superficial velocity in Figure (4.9) as:

$$Sh_g \propto Re_g^{0.41} \quad \ldots\ldots\ldots (4.9)$$

The physical properties of the electrolyte solution has been used to define the dimensionless number (Sh) because the electrochemical reactions occur at solid/liquid interphase and depend on the concentration of electrolyte. Other parameters such as velocity and characteristic length are of course the superficial velocity of gas since the increase in gas flow rate enables the mass transfer rate at the electrode surface. Equation (4.9) can be compared with the studies of Walker and Wragg (1980) for rectangular duct:

$$Sh \propto Re^{0.54} \quad \ldots\ldots\ldots\ldots (4.10)$$

The knowledge of the fraction of gas present in the system and average bubble diameter is important in

60
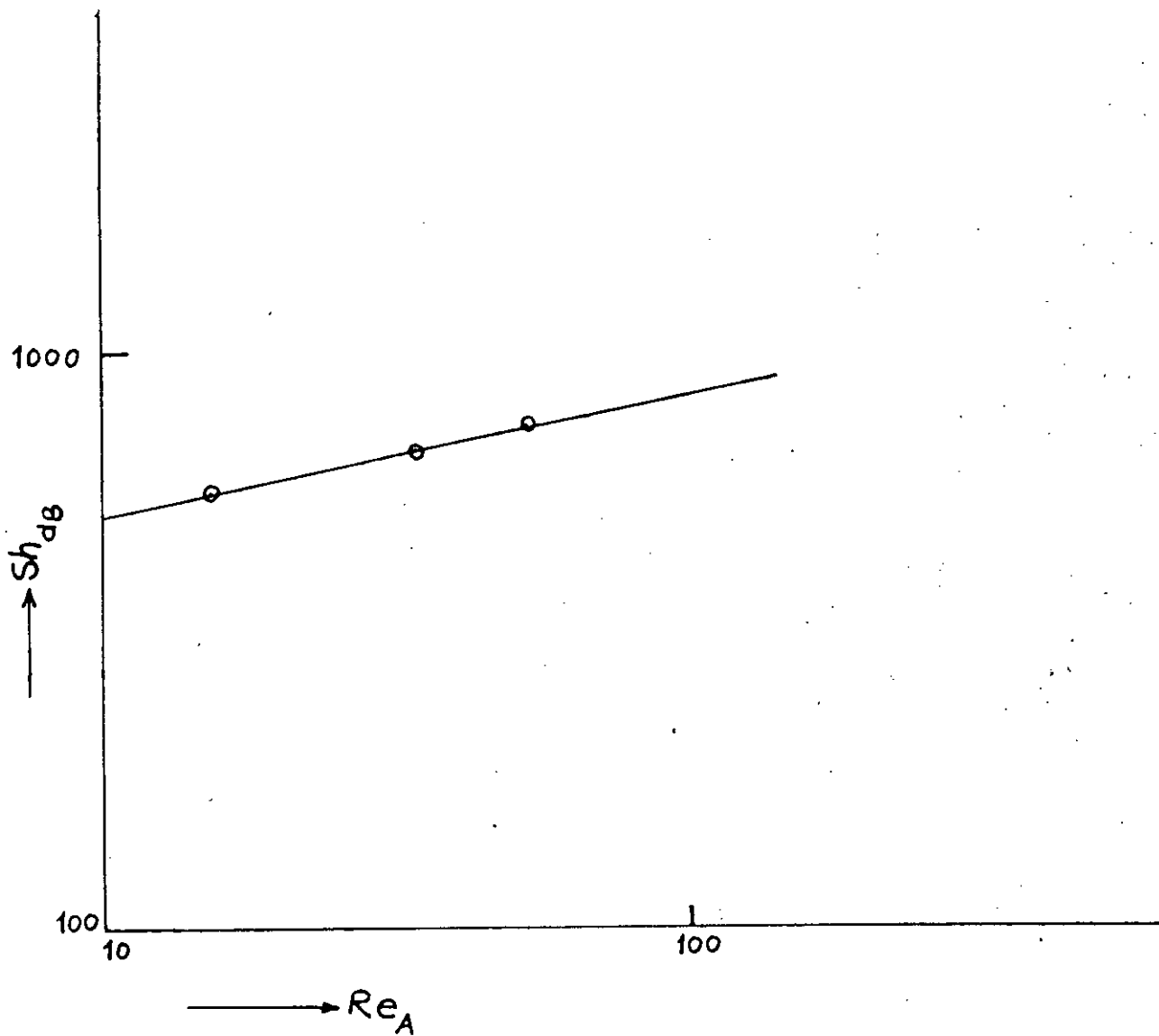
FIGURE 4-10 Sh_{dB} versus Re_A

establishing the overall mass transfer correlation. The real mass transfer processes at gas evolving electrodes can be represented from the logarithmic plot of Sherwood number against Reynolds number based on average bubble rise diameter as shown in Figure 4.10:

$$Sh_{dB} \propto Re_A^{0.21} \quad \ldots\ldots\ldots\ldots(4.11)$$

Equation (4.10) can be compared with mathematical model presented by Vogt and Stephan (1979) as well as Ali (1982) which gives:

$$Sh_{dB} \propto Re_{dB}^{0.5} \quad \ldots\ldots\ldots\ldots(4.12)$$

4.5.1. CURRENT DISTRIBUTION AND MASS TRANSFER RATE IN SIMULTANEOUS GAS-LIQUID FLOW SYSTEM

The results in the study of the deposition of copper from copper sulphate- sulphuric acid solution by forced circulation of electrolyte with simultaneous passing of gas bubbles was obtained in a similar way as reported before for gas sparging. The electrolyte flow rate was varied from 4.4 lit/min to 7.8 lit/min and gas flow rate from 5.0 lit/min to 8.2 lit/min.

The bubble size distribution, average bubble diameter and the volume fraction of gas present in the solution have also been studied to obtain mass transfer correlation for this system and these have been compared with correlation

61
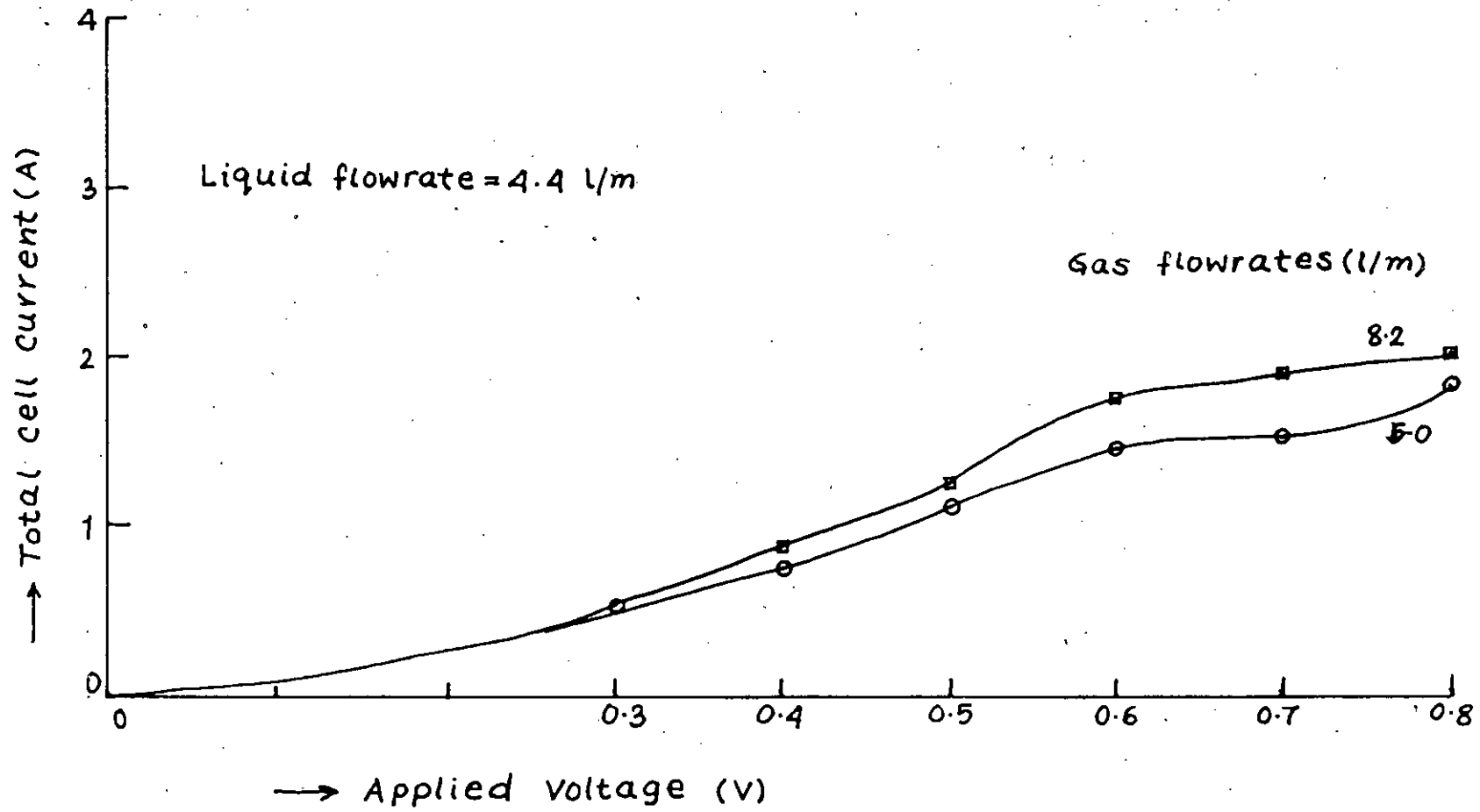
FIGURE 4-11   CURRENT-VOLTAGE CURVE AT DIFFERENT GAS FLOWRATES
WITH CONSTANT LIQUID FLOWRATE
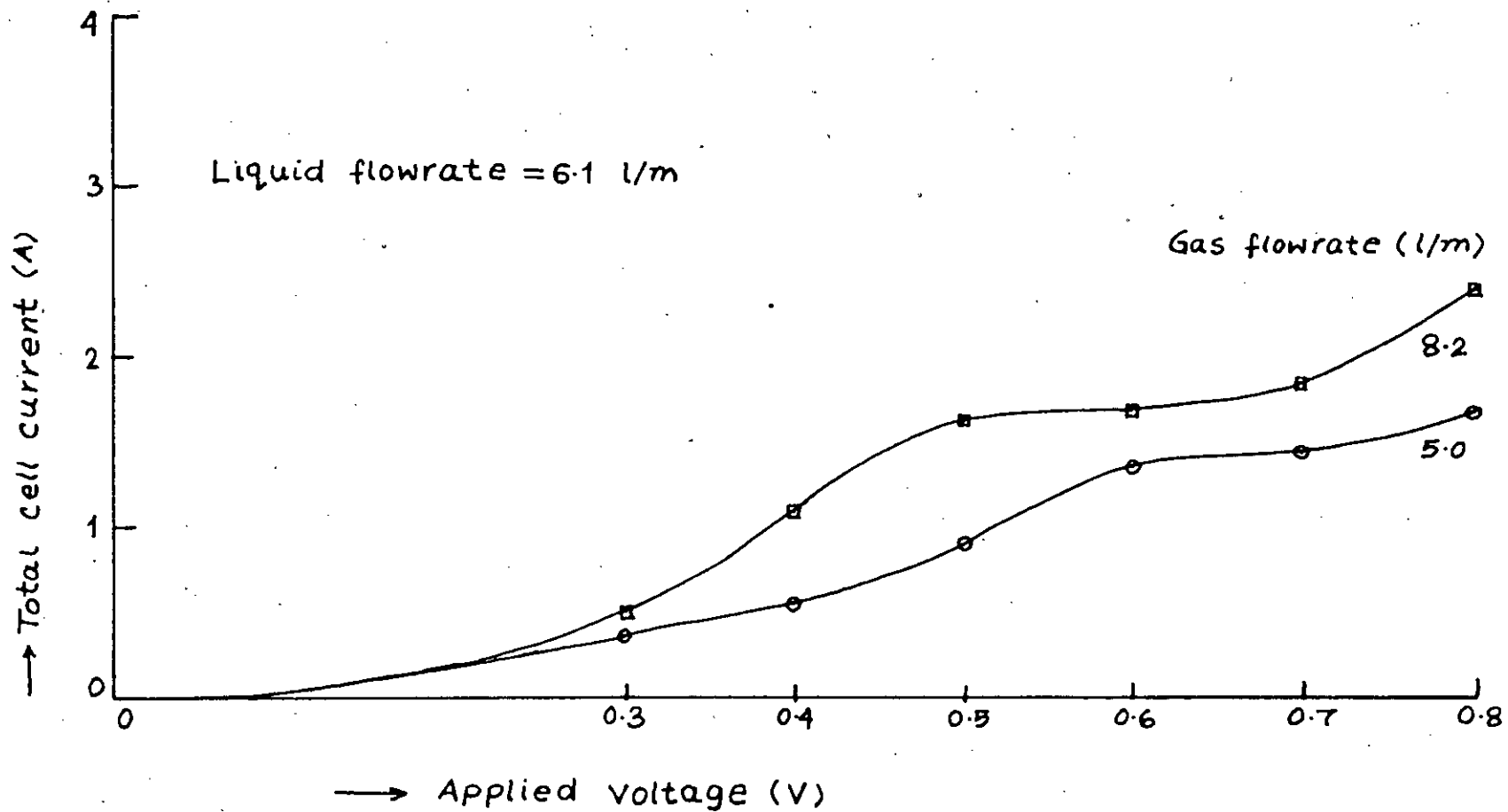
FIGURE 4-12   CURRENT-VOLTAGE CURVE at different r

GAS FLOWRATE WITH CONSTANT LIQUID FLOWRATE
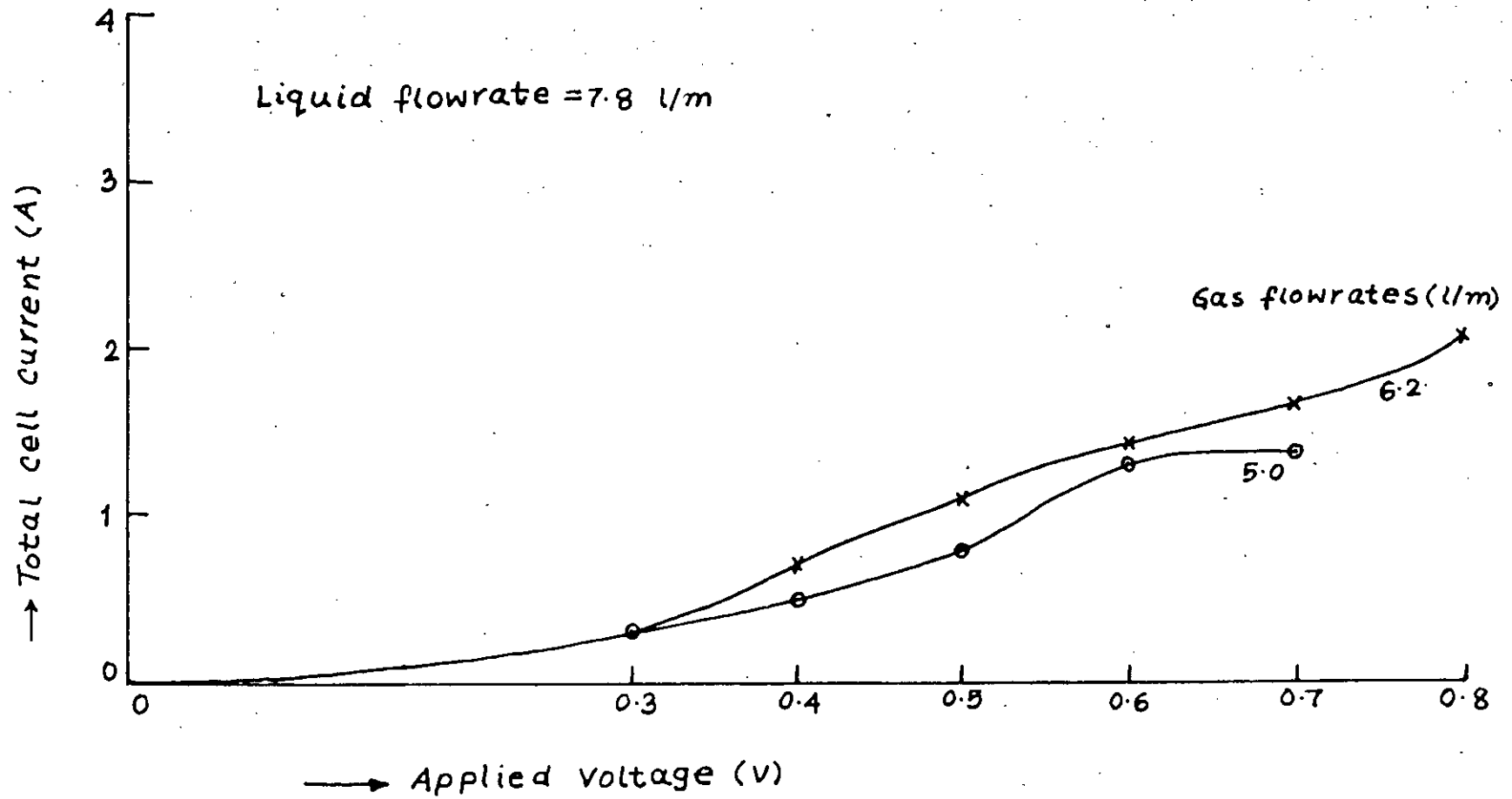
FIGURE 4-13   CURRENT-VOLTAGE CURVE AT DIFFERENT GAS FLOWRATE

WITH CONSTANT LIQUID FLOWRATE

obtained before using gas sparging through stationary solution and other correlations obtained from relevant gas/liquid systems.

As before the total cell current against the applied voltage has been drawn in Figures 4.11, 4.12 and 4.13 for various electrolyte flow rate with simultaneous flow of gas. Each figure shows the curves at a constant liquid flow rate with two different gas flow rates. Table 4.3 gives the summary of electrolyte and gas flow rates that have been used:

TABLE 4.3   DIFFERENT SET OF GAS-LIQUID FLOW RATE USED

	Liquid flow rate	Gas flow rate
Figure 4-11	4.4 lit/min	5.0 and 8.2 lit/min
Figure 4-12	6.1 lit/min	5.0 and 8.2 lit/min
Figure 4-13	7.8 lit/min	5.0 and 6.5 lit/min

The minimum flow rate of gas used in this study was 5.0 lit/min because the lower flow rate of gas supply was unsteady due to the pressure exerted by the electrolyte at the mouth of the air sparger.

The total current calculated from the summation of individual current on the cathode sections were found to be in good agreement with the measured total current

specially at the limiting conditions where the two values were very close. Runs were repeated to check the reproducibility which was achieved and the results were reported in Appendix D.

From the current-voltage curve, it has been found that the limiting current plateau varies from 100 mV (in most cases) to 200 mV (liquid flow rate=6.1 lit/min, gas flow rate=8.2 lit/min) with slight inclination. The starting point of limiting current plateau varies from 500 mV to 600 mV. The shift in starting point of limiting conditions is largely due to the solution voltage drop at higher current at limiting conditions and higher activation overpotential. The value of the limiting current obtained in the present system lie below those obtained using gas sparging through stationary solution. For a given liquid flow rate, the value of limiting current increases with the increase in gas flow rate. This means that in the presence of electrolyte flow, the intensity of turbulence increases at the electrode surface with the increase in gas flow as found for gas sparging in stationary electrolyte but at a reduced rate.

The current distributions in this system have been presented graphically in the form of histograms as the fraction of total current passing through the sections

Liquid flowrate = 6·1 l/m
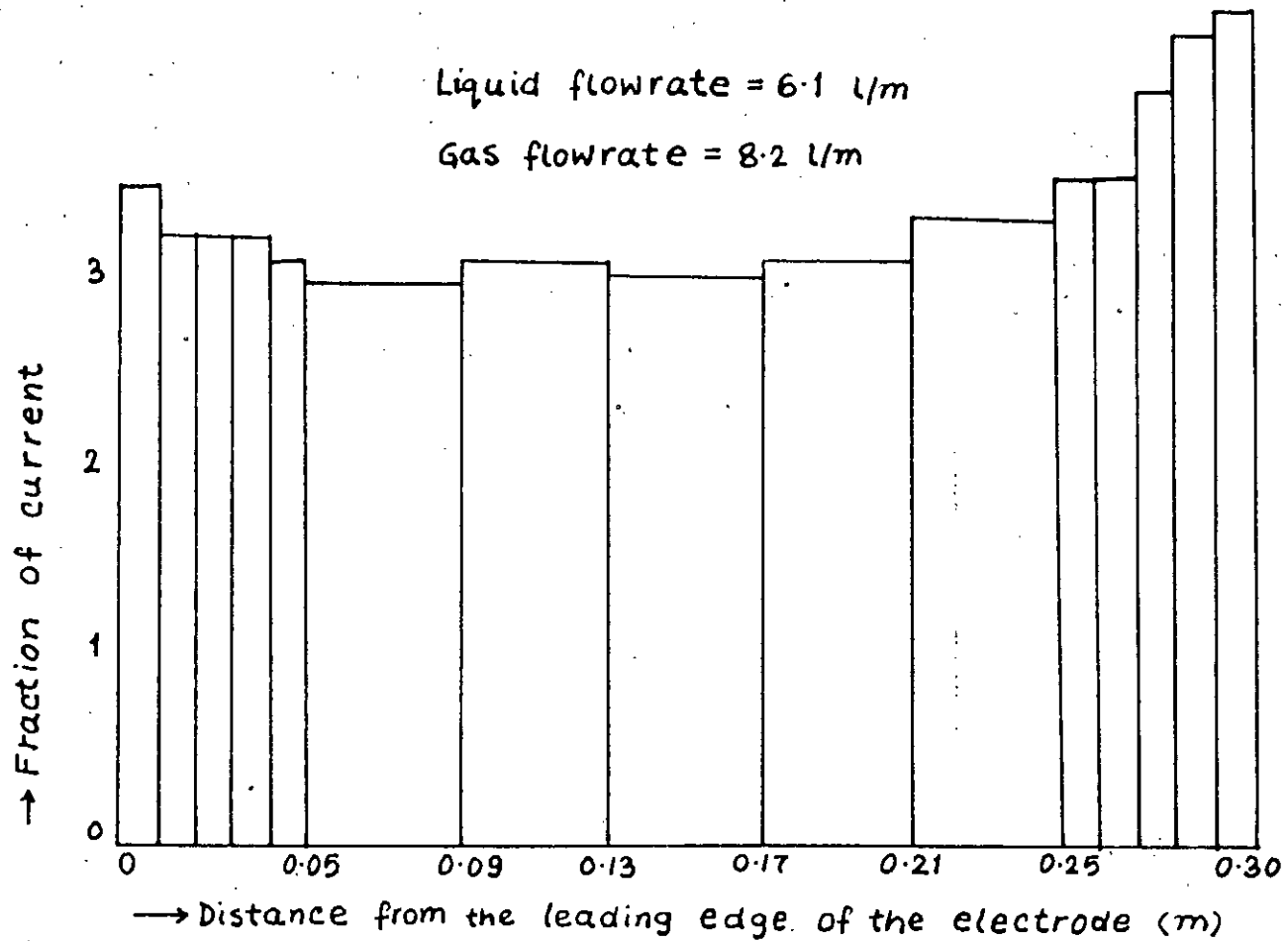
Gas flowrate = 8·2 l/m

FIGURE 4-14   FRACTION OF CURRENT AT DIFFERENT SECTIONS

AT DIFFERENT LIQUID AND GAS FLOWRATE
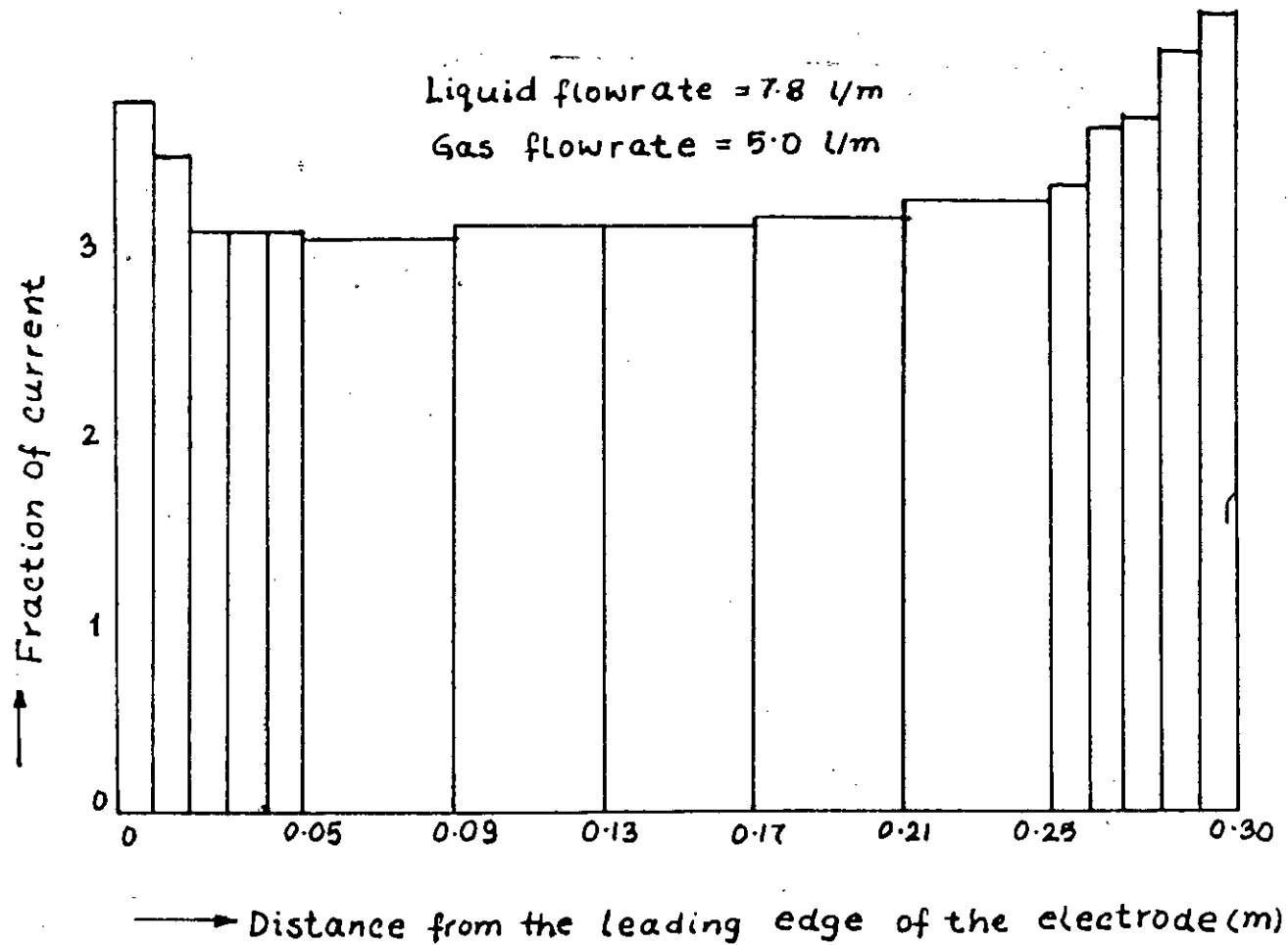
FIGURE 4-15   FRACTION OF CURRENT AT DIFFERENT

SECTIONS AT DIFFERENT LIQUID AND GAS FLOWRATE

of the electrode under limiting current conditions. The current distributions in the two phase flow system can roughly be defined as consisting of three regions as shown in Figures 4-14 and 4-15. The three regions are the inlet, the mid sections and the exit. The lowest current passes through the mid sections of the cell covering a length of 20 cm in total, but in Figure 4-14 the mid section covered from segment 5 to segment 9 with a length of 17 cm and in Figure 4-15, from segment 3 to segment 11 with a total length of 24 cm based on the lowest current. The current distribution at the exit section was higher than that of the entrance section. Both Figures 4-14 and 4-15 show that the highest current passes through the last sections of the sections of the cathode which was due to the acceleration of both gas and electrolyte at the exit sections of the cathode. The distributions were similar to those of gas sparging in stationary solutions but the only difference is that the ratio of current at the entrance sections to that of the mid sections was smaller in the present system.Thus the current distribution was more uniform in simultaneous gas-liquid flow than gas sparging only.

Since the variation of mass transfer coefficients on individual sections are reflected in the variation of current distribution as shown in Figures 4-14 and 4-15,

Mass transfer coefficient (m/s) × 10⁵ (y-axis)

Flow rate (l/m) (x-axis)

Gas sparging only

Constant liquid flow at different gas flowrates

4.4
6.1
7.8
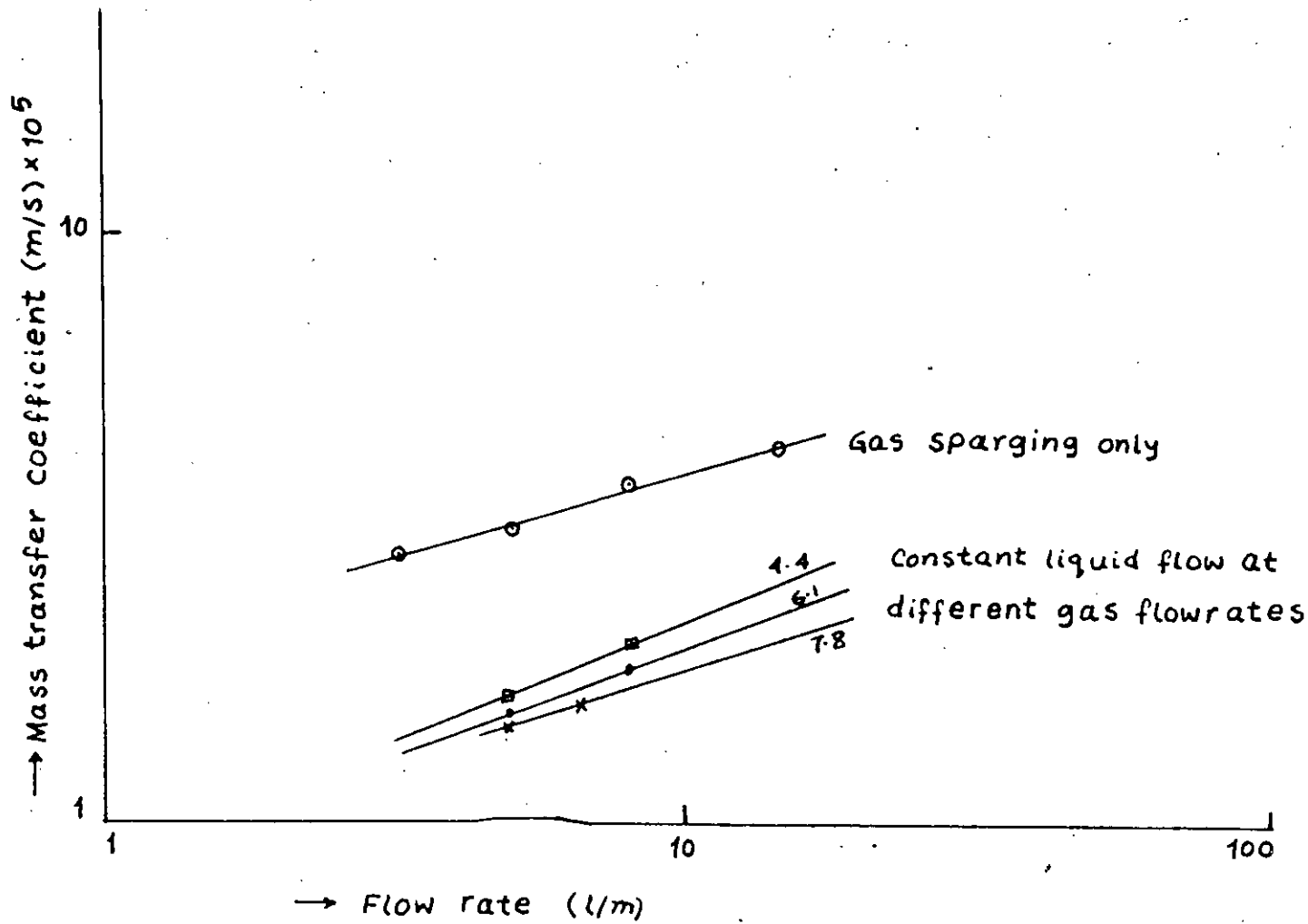
FIGURE 4-16   COMPARISON OF MASS TRANSFER COEFFICIENT

BY DIFFERENT MODES OF CONVECTION

it can be concluded that the individual mass transfer coefficient is more uniform along the length of the electrode.

4.5.2. MASS TRANSFER CORRELATION IN CASE OF TWO PHASE FLOW

The overall mass transfer coefficients have been calculated from the measured total current at limiting conditions from the current-voltage curves in Figures 4-11 to 4-13. These have been presented logarithmically against superficial velocity of gas at different electrolyte flow rates in Figure 4-16 along with the mass transfer coefficient obtained using gas sparging only for comparison purposes. It shows that at a constant electrolyte flow rate, the mass transfer rate increases with increasing superficial gas velocity. For all electrolyte flow rates the mass transfer coefficient rises in similar fashion with the increase in gas flow rate and the exponent on the superficial velocity of gas is approximately 0.4 which was same in case of gas sparging only.

Figure 4-16 also shows that the mass transfer enhancement resulting from gas sparging through stationary solution is higher than that caused by simultaneous gas liquid flow and mass transfer rate increases with decrease in

65
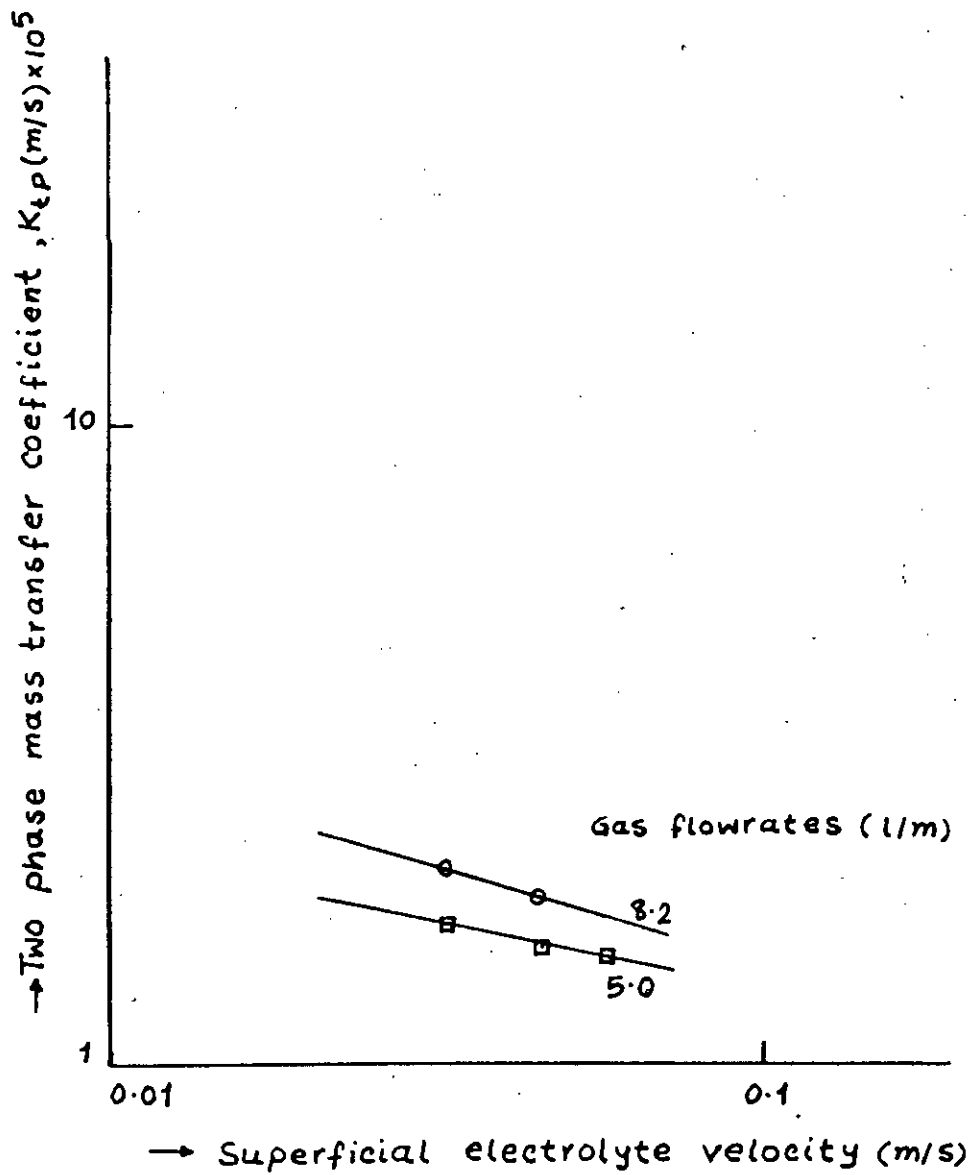
FIGURE 4-17   TWO PHASE MASS TRANSFER

COEFFICIENT WITH ELECTROLYTE VELOCITY AT

CONSTANT GAS FLOWRATE

electrolyte flow in case of simultaneous gas electrolyte flow. These finding agrees with the experimental study of Sigrist et el (1979) and Ali (1982).

Figure 4-17 shows that the variation of mass transfer coefficient at different superficial electrolyte velocity at constant superficial gas velocity. It shows that for a given gas velocity the mass transfer rate decreases with the increase in electrolyte flow and the exponent on the superficial electrolyte velocity is about - 0.2. The reason is due to the flow of liquid carrying bubbles in the direction of the axis of the flow rather than assisting the creation of turbulence at the electrode surface by the transverse motion of the electrolyte. As the flow rate of the electrolyte increases, the superimposed fluid flow increases the rising velocity of the bubble which in turn results in bubble expansion and reduces the influence of gas flow on the mass transfer rate in two-phase flow as the liquid flow rate increases, (The volume fraction of gas present in the system increases as the flow rate of electrolyte increases). Since the variation of two phase mass transfer coefficients (K_{tp}) with superficial velocity of gas and liquid are obtained separately, they have been combined together to obtain a suitable correlation. k_{tp} has been plotted against ($U_g^{0.4}/U_l^{0.2}$) in a logarithmic
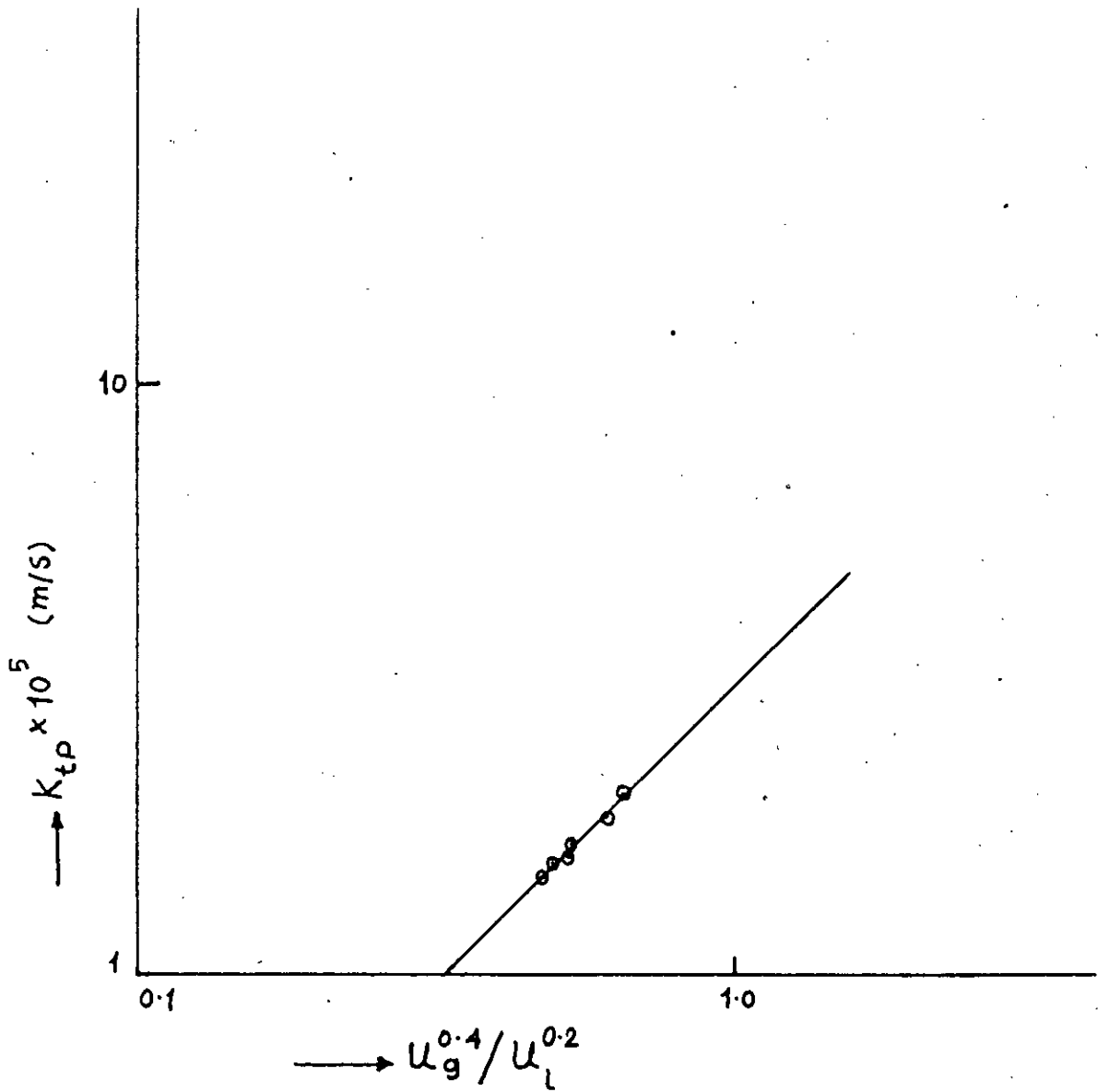
FIGURE 4-18 K_{tp} VERSUS $U_g^{0.4}/U_l^{0.2}$

plot in Figure 4-18 and the slope of this curve is about unity giving the following correlation for the present study:

$$K_{tp} = 2.08 \times 10^{-5} \ \frac{U_g^{0.4}}{U_1^{0.2}} \qquad \ldots\ldots(4.13)$$

or alternatively, by inferring a $Sc^{1/3}$ proportionality to K_{tp} :

$$K_{tp} \ Sc^{1/3} = 0.0124 \ U_g^{0.4} \ (U_g/U_1)^{0.2} \quad \ldots.(4.14)$$

A Similar expression has been obtained by Ali (1982) using the same simultaneous gas liquid flow in a reactor having similar geometrical shape.

The dependence of overall mass transfer rate on the superficial velocity of gas and liquid has been obtained, but useful correlations are also possible if the bubble diameters and the void fractions of gas present in the system are known. Photographs of bubble size distribution at different gas-electrolyte flow rate have been shown in Plates 4-3 and 4-4. The bubbles are distributed over most regions of the reactor and the coalescence of the bubbles are less than that in gas sparging only. Table 4.4 shows the average bubble diameter and void fraction at different flow rates calculated from the photographs in a similar procedure used in gas sparging through stationary electrolyte.
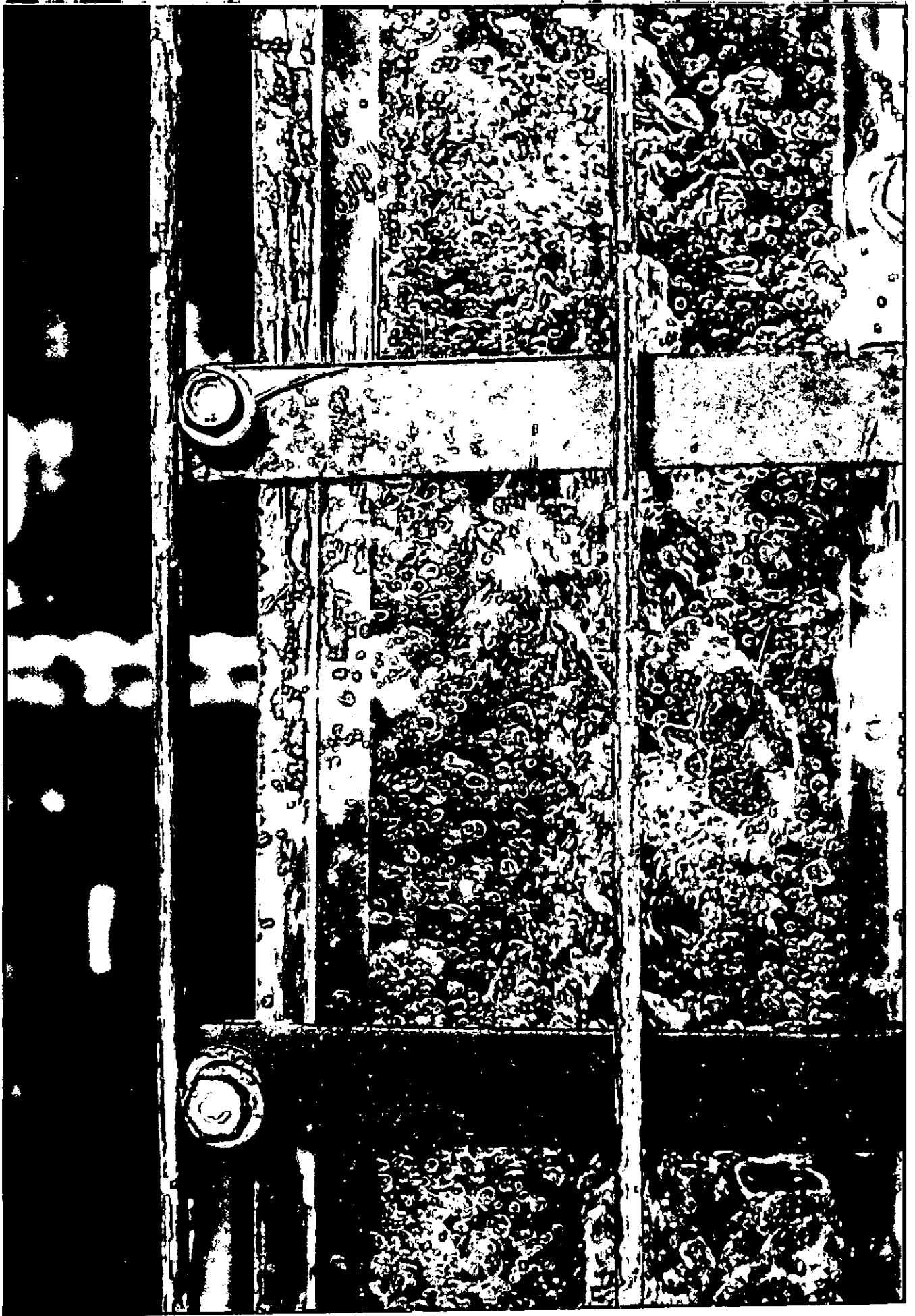
PLATE 4-3 : GAS FLOW RATE = 5.0 lit/min, LIQUID FLOW RATE=6.1 lit/min.
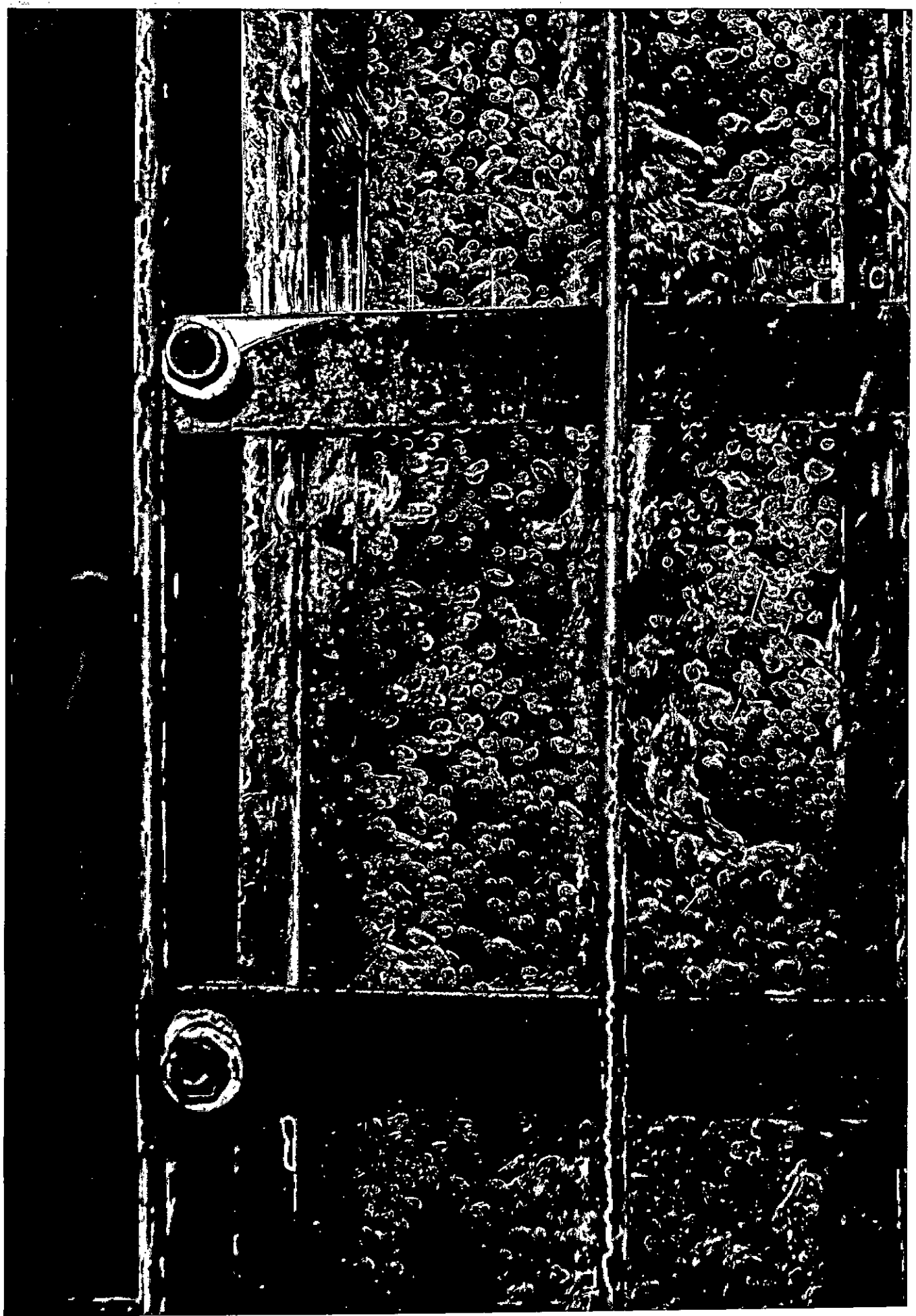
PLATE 4-4: GAS FLOW RATE = 8.2 lit/min, LIQUID FLOW RATE = 4.4 lit/min.

TABLE 4.4   BUBBLE DIAMETER

Liquid flow rate (lit/min)	Gas flow rate (lit/min)	average bubble diameter (mm)	void fraction
6.2	5.0	6.26	0.050
4.4	8.2	6.71	0.082

Table 4.4 shows that the average bubble diameter is more or less constant at different gas electrolyte flow rate and void fraction is below 0.2. but volume fraction of gas present in the two phase flow dispersion system can be determined accurately from the solution conductivity measurement.

CONCLUSIONS AND SUGGESTIONS

An analysis of the results obtained from the present study of mass transfer rates for the deposition of copper at different sections of the cathode with different convective systems leads to the following inferences to be made:

1. All the sections of the cathode attained limiting current conditions more or less simultaneously for a range of applied potential for all the convective modes. The starting point of limiting current condition varied between 500 to 600 mV.

2. The maximum mass tranfer rates occured adjacent to the flow inlet and exit regions due to the hydrodynamic entrance and exit effects. For two phase flow, the maximum mass transfer was observed at the exit region.

3. The value of mass transfer rate decreases with the distance from the reactor entrance and rises again at the outlet sections. The cumulative average mass transfer coefficient in these regimes have been related to L/D_e as $K_{avg} \propto L/D_e^{-0.10}$.

4.   The overall mass transfer rate for gas sparging through stationary electrolyte is much higher than the simultaneous gas-liquid flow. The mass transfer rate for simultaneous flow system increases with the increase in gas flow at constant liquid flow rate but decreases with the increase in liquid flow rate at constant gas flow.

5.   The average bubble diameter as well as the volume fraction of gas present in the solution increases with increase in gas flow rate in the case of gas sparging only.

6.   The overall mass transfer correlation obtained for gas sparging is:

$$Sh = 0.015 \ Re^{0.41} \ Sc^{1/3}$$

7.   For two-phase flow an overall mass transfer correlation was derived as:

$$K_{tp} = 2.08 \times 10^{-5} \ (U_g^{0.4}/U_l^{0.2}) \ .$$

The following suggestions may be applicable for further work :

1.   Studies can be carried out using different cell geometry and different electrode sizes.

70

2. Void fraction can be determined accurately by conductivity measurement for gas sparging and simultaneous gas-liquid flow.

3. Bubble diameter can be determined more accurately by using bubble size analyzer.

4. Different convective mode can be used for determining mass transfer during electrodeposition.

REFERENCES

1. GENDRON, A.S. and ETTEL, V.S. Can. J. Chem. Eng. 53, 36, (1975).

2. ALI, M.S. Ph. D Thesis, University of Manchester,(1982).

3. AHMED, M.; M.Sc. Thesis, University of Engineering & Technology, (1984).

4. De La RUE, R.M. and TOBIAS, C.W. J. Electrochem. Soc., 106, 827, (1959).

5. SIGRIST, L., DOSSENBACH, O. and IBL, N. Int. J. Heat and Mass Transfer, Vol.22,1393,(1979).

6. LEIBSON, I., HOLCOMB, E.G., CACOSA, A.G. and JACMIE, J.J. A.I.Ch.E.J., 2, 296, (1956).

7. IBL, N., KIND, R. and ADAM, E. Ann. Chem., 71, 1008, (1975).

8. IBL, N. Chem. Eng. Tech. 43, 202, (1971).

9. JANSSEN, L.J.J. and HOOGLAND, J.G. Electrochimica Acta, 15, 1013, (1970).

10. SEDAHMED, G.H. J. Appl. Electrochem. Soc., 8, 399, (1978).

11. MOHANTA, S. and FAHIDY, T.Z. 7, 235, (1977).

12. STEPHAN, K. and VOGT, H. Electrochimica Acta, 24, 11, (1979).

13. VOGT, H. Electrochimica Acta, 23, 1019, (1978).

14. ROWE, P.N., CLAXTON, K.T. and LEWIS, J.B. Trans. Inst. Chem. Engrs., 43, 114, (1965).

15. CALDERBANK, P.H. Trans. Inst. Chem. Engrs., $\underline{37}$, 173, (1959).

16. JENNINGS, D., KUHN, A.T., STEPANEK, J.B. and WHITEHEAD, R. Electrochimica Acta, $\underline{20}$, 903, (1975).

17. VOGEL, A.I. "A Textbook of Quantitative Inorganic Analysis" 3rd Edition, Longmans, (1961).

18. JABBAR, A.M., and HAQUE, M.M. "Practical Chemistry", 2nd Edition, Student Ways, Bangladesh, 1972.

NOMENCLATURE

A_e Electrode area, m².

Ar^* Archimedes number.

C_i Concentration of the species i

D_i Diffusion coefficient of the species i, m²/s.

d_B Bubble diameter, m.

d_o Orifice diameter, m.

d_{vs} Volume to surface diameter of the bubble, m.

F Faraday constant.

f Void fraction.

K_g Liquid phase mass transfer coefficient, m/s.

K_{tp} Two phase mass transfer coefficient, m/s.

k_{gl} Conductivity of gas-liquid dispersed phase.

k_l Conductivity of gas free solution.

k_d Conductivity of dispersed phase.

K_{avg} Average mas transfer coefficient, m/s.

N_i Molar flux of the species i.

Re_o Reynolds number at the orifice.

Re_g Liquid phase Reynolds number during gas sparging through stationary electrolyte.

Re_{dB} Reynolds number based on bubble diameter.

Sc Schmidt number.

Sh_{dB} Sherwood number based on bubble diameter.

Sh, Sh_g	Liquid phase sherwood number during gas sparging through stationary electrolyte.
U	Velocity of the electrolyte, m/s.
u_g	Superficial gas velocity, m/s.
u_s	Slip or relative velocity between gas and liquid, m/s.
u_t	Air bubble terminal velocity, m/s.
u_1	Superficial liquid velocity, m/s.
V_g	Rate of gas evolution, litre/s.
Z_i	Valency of the species i.

APPENDIX   A

CELL   DIMENSIONS   AND   PHYSICAL   PROPERTIES   OF   COPPER

SULPHATE IN SULPHURIC ACID AND OTHER RELEVANT DATA

The physical properties of 0.015 copper sulphate in 1.5

M sulphuric acid has been taken from Stanmore (1970) and

Wilson (1974). They collected the data from several

sources. For the present study, the concentration

variations during the different experimental runs were

very negligible and the concentration of copper sulphate

was considered constant. Similarly, the temperature of

the solution was always maintained at $(30\pm2)^\circ$ C. The

density, viscosity and diffusivity of 0.015 M copper

sulphate in 1.5 M sulphuric acid used are as follows:

Density (ρ) = 1.091 $\times$ 10^3 Kg/m^3.

Viscosity (μ) = 1.22*10^{-3} Kg/(m)(s)

Diffusivity (D) = 5.15*10^{-10} m^2/s

Schmidt number (Sc) = 2171

Density of Nitrogen = 1.25 Kg/m^3.

The same cell was used in all experimental works and the cell dimensions are as follows:

Length of the electrodes (L) = 0.3 m

Width of the electrodes (W) = 0.11 m

Spacing between the electrodes (s) = 0.02 m

Equivalent diameter (d_e)

$$= 4WS/2(W+S)$$

$$= 4*0.11*0.02/\{2(0.11+0.02)\}$$

$$= 0.0338 \text{ m}$$

Aspect ratio (S/W) = 0.02/0.11 = 0.18

Total electrode area = 0.3*0.11 = 0.033 m^2

Cross sectional area for flow = 0.11*0.02 = 0.0022 m^2

APPENDIX   B

FLOW CALIBRATION CURVES FOR ROTAMETERS USED IN THE

EXPERIMENT

This appendix presents the rotameter calibration
curves for liquid (0.015 M copper sulphate in 1.5
M sulphuric acid) and gas (oxygen free nitrogen).
The rotameter calibration curve for liquid flowrate
measurement was drawn from calibration data obtained
through experiments.The rotameter for gas flowrate
measurement was calibrated using soap-bubble
method.

The calibration curves are presented in Figures B.1
and B.2.
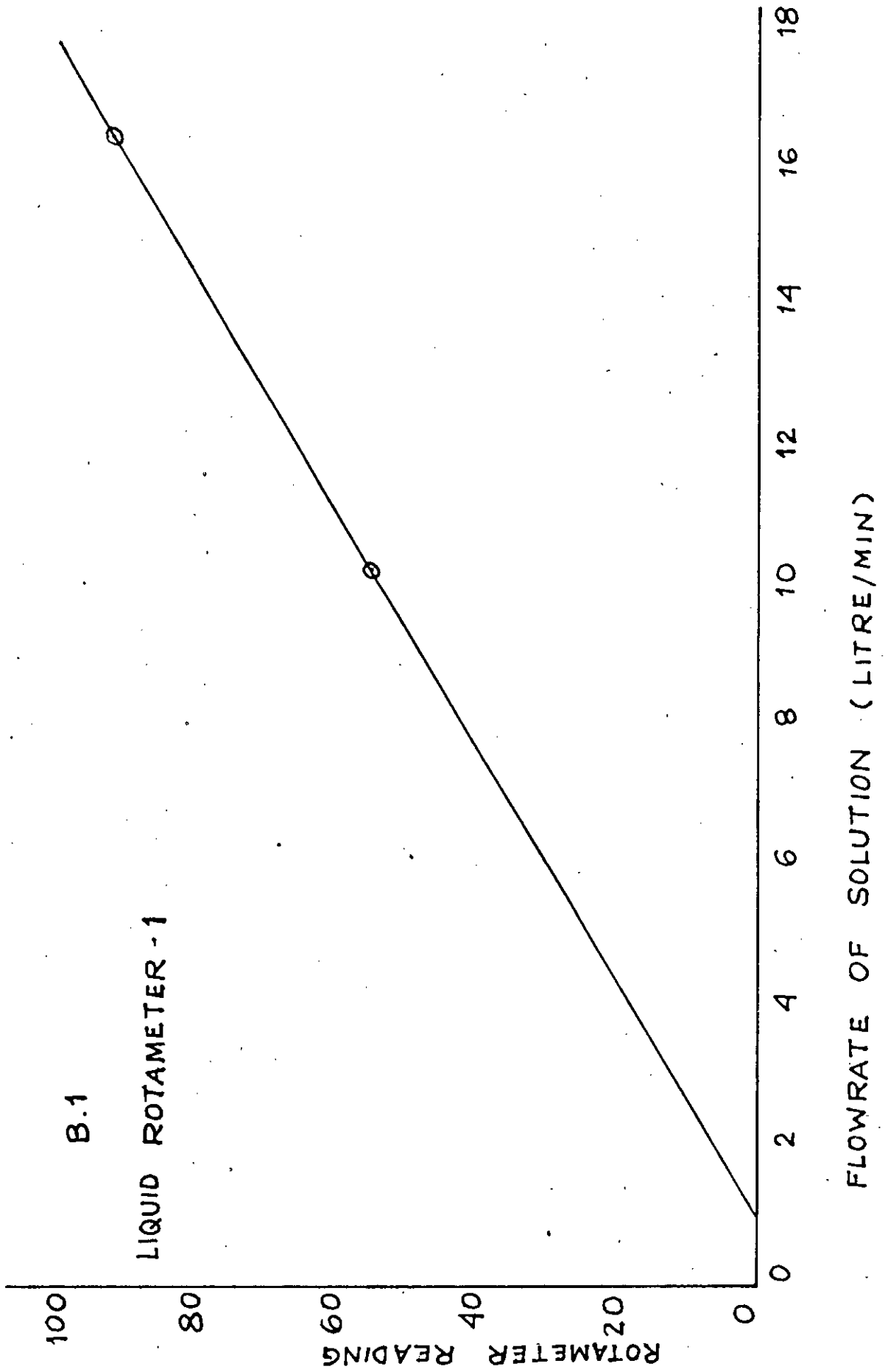
B.1

LIQUID ROTAMETER-1

ROTAMETER READING

FLOWRATE OF SOLUTION (LITRE/MIN)

B.2 GAS ROTAMETER
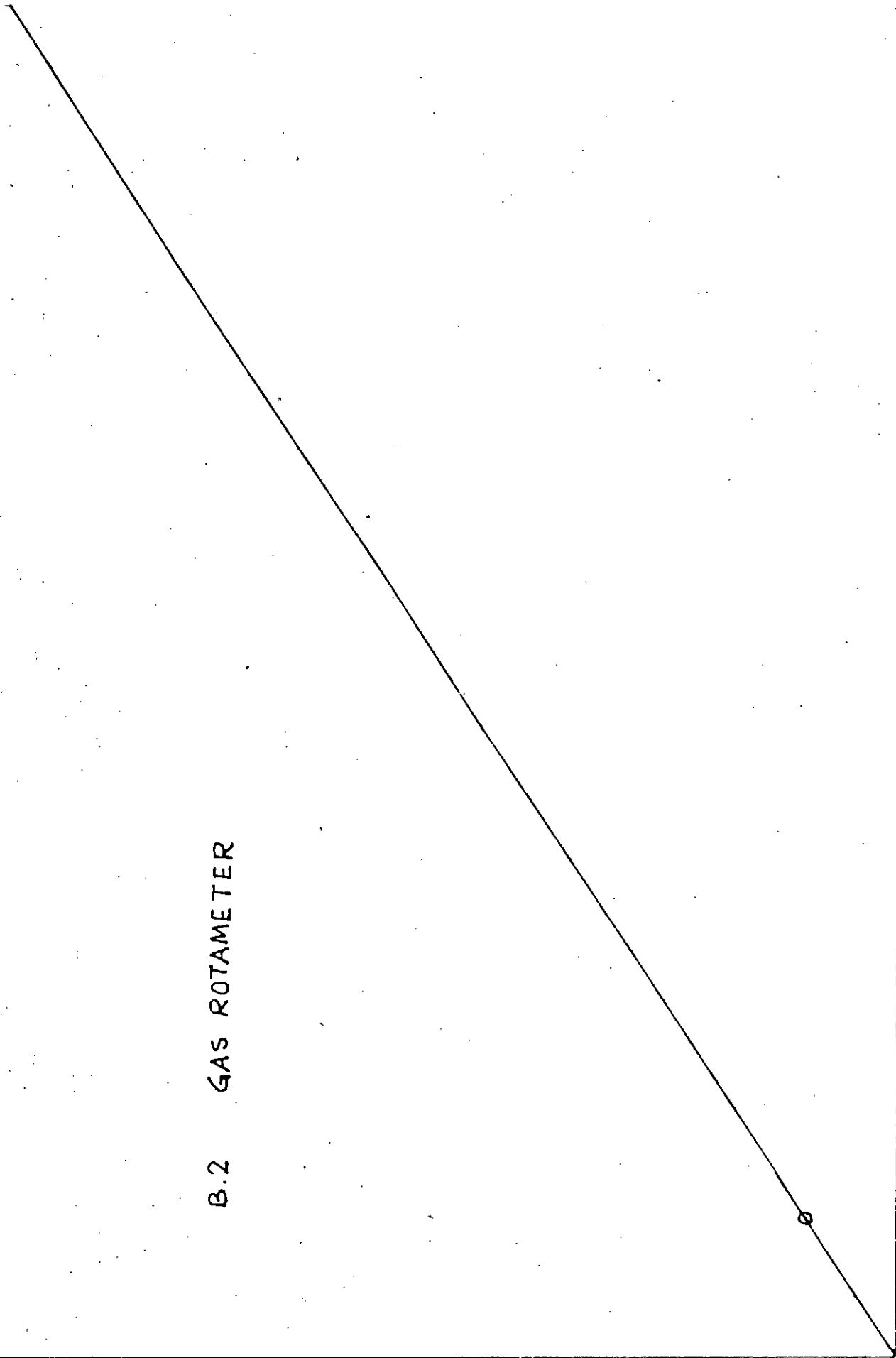
APPENDIX   C

EXPERIMENTAL CURRENT-VOLTAGE DATA AND CALCULATED RESULTS

FOR GAS SPARGING THROUGH STATIONARY SOLUTION

C.1　　　　　Gas Flowrate = 1.65 lit/min

Current distribution at different cathode sections

Cathode Section	Applied Voltage(mV)	200	300	400	500	600	700
1		9.5	25	53	75	85	105
2		9.5	22	48	70	80	
3		8.0	20	45	65	70	
4		7.0	18	45	65	70	
5		7.0	18	42	60	70	
6		27	70	160	230	255	290
7		24	70	155	220	240	
8		24	70	155	220	230	
9		26	70	160	215	230	
10		26	65	155	220	235	
11		7.0	16	40	60	60	
12		7.5	16	42	60	70	
13		7.5	17	44	60	65	
14		7.5	19	46	65	70	
15		7.5	19	46	65	75	
Total Measured Current (mA)		225	535	1275	1810	1955	
Total Current Accounted (mA)		204	492	1234	1750	1910	

C.2   Gas Flowrate = 3.25 lit/min

Current distribution at different cathode sections

Cathode Section	Applied Voltage(mV)	200	300	400	500	600	700
1		10	30	55	80	98	105
2		10	25	50	76	92	100
3		9	25	50	72	86	96
4		8.5	24	47	72	94	95
5		8.5	24	48	70	89	95
6		28	80	182	242	323	355
7		28	75	174	242	327	340
8		27	75	178	239	320	340
9		27	75	175	235	320	350
10		27	80	179	235	324	350
11		8.0	22	45	71	86	92
12		8.5	22	48	71	85	92
13		8.5	23	49	74	89	92
14		9.0	25	52	75	89	95
15		9.0	30	52	75	93	97
Total Measured Current (mA)		285	690	1440	2055	2620	2730
Total Current Accounted (mA)		226.5	635	1384	1929	2513	2695

C.3   Gas Flowrate = 5.80 lit/min

Current distribution at different cathode sections

Cathode Section	Applied Voltage(mV)	200	300	400	500	600	700
1		11	49	72	94	115	124
2		11	45	68	94	112	124
3		9.5	48	68	90	112	121
4		10	48	64	88	111	122
5		10	46	65	87	109	119
6		33	164	240	280	355	374
7		32	164	235	276	351	363
8		33	164	236	276	344	353
9		30	168	236	268	343	352
10		30	165	234	275	350	355
11		8.5	40	62	88	106	117
12		9	44	65	88	107	118
13		9	49	65	92	110	122
14		10	48	69	94	114	122
15		10	48	70	95	114	124
Total Measured Current (mA)		310	1385	1930	2480	3020	3165
Total Current Accounted (mA)		256	1290	1849	2346	2853	3010

C.4   Gas Flowrate = 8.20 lit/min

Current distribution at different cathode sections

Cathode Section	Applied Voltage(mV)	200	300	400	500	600	700	800
1		14	59	94	120	142	155	179
2		12	59	92	117	137	148	179
3		11	55	89	115	137	143	170
4		10.5	53	89	115	134	149	177
5		10	54	88	115	136	142	162
6		38	204	330	378	399	432	452
7		38	197	330	373	410	425	437
8		36	186	324	370	407	422	438
9		36	186	325	372	418	423	455
10		37	190	325	375	416	429	463
11		10	52	87	114	134	142	170
12		11.5	52	87	114	135	145	172
13		13	57	93	116	135	145	171
14		13	58	93	118	137	149	174
15		14	58	93	118	138	158	174
Total Measured Current (mA)		405	1600	2710	3250	3525	3607	3973
Total Current Accounted (mA)		304	1520	2539	3030	3415	3594	3908

C.5   Gas Flowrate = 9.90 lit/min

Current distribution at different cathode sections

Cathode Section	Applied Voltage(mV)	200	300	400	500	600	700	800
1		18	64	117	145	183	205	224
2		18	60	114	142	179	201	221
3		16	58	114	139	176	203	219
4		13	55	111	139	180	198	215
5		13	56	110	138	180	195	215
6		42	200	396	460	466	538	572
7		44	206	392	456	472	524	556
8		44	202	389	450	470	535	564
9		43	195	394	448	465	530	568
10		46	198	394	452	476	529	565
11		12	53	110	135	180	194	216
12		14	53	109	138	177	194	218
13		15	54	112	140	185	197	219
14		15	59	115	144	182	200	219
15		18	61	118	144	185	204	224
Total Measured Current (mA)		445	1640	3230	3825	4395	4835	5400
Total Current Accounted (mA)		371	1577	3095	3670	4155	4647	5015

C.6   Gas Flowrate = 11.5 lit/min

Current distribution at different cathode sections

Cathode Section	Applied Voltage(mV)	200	300	400	500	600	700	800
1		22	69	120	152	198	205	223
2		22	68	117	155	201	205	220
3		18	65	117	150	194	198	210
4		16	65	115	146	196	197	214
5		16	63	114	144	196	199	216
6		65	214	401	500	453	480	570
7		59	208	398	590	442	492	559
8		62	208	388	494	448	478	564
9		65	210	397	507	450	496	554
10		67	210	395	505	440	496	566
11		18	60	114	142	195	195	215
12		18	61	114	140	194	203	218
13		20	64	114	148	194	207	218
14		21	64	116	149	197	200	222
15		22	68	121	151	198	204	223
Total Measured Current (mA)		580	1885	3350	4280	4530	4900	5650
Total Current Accounted (mA)		511	1694	3141	3973	4196	4453	4992

C.7   Gas Flowrate = 14.65 lit/min

Current distribution at different cathode sections

Cathode Section	Applied Voltage(mV)	200	300	400	500	600	700	800
1		25	74	137	172	180	218	198
2		25	72	134	163	175	210	195
3		22	68	132	159	171	220	
4		19	66	132	156	170	215	
5		18	65	128	156	168	200	
6		76	218	411	530	529	557	
7		72	214	398	519	520	542	
8		64	209	395	514	520	571	
9		63	212	403	514	524	536	
10		71	212	412	523	520	565	
11		20	64	126	152	158	177	
12		20	69	127	154	160	192	
13		23	69	130	157	169	192	
14		22	70	135	161	169	204	
15		25	73	135	168	174	211	
Total Measured Current (mA)		650	1975	3590	4520	4700	5410	
Total Current Accounted (mA)		565	1755	3335	4198	4308	4810	

C.8   Calculation of mass transfer coefficient in each section
       at limiting current (K_{av} at each section $\times 10^5$ m^2/s)

Section	Gas Flowrate (lit/min)			
	3.25	5.8	8.2	14.65
1	3.297	3.894	4.867	5.652
2	3.140	3.894	4.648	5.495
3	3.015	3.800	4.491	5.370
4	2.983	3.831	4.679	5.338
5	2.983	3.737	4.459	5.276
6	11.148	11.744	13.566	16.611
7	10.677	11.399	13.346	16.330
8	10.677	11.085	13.252	16.332
9	10.991	11.054	13.283	17.400
10	10.991	11.148	13.472	16.329
11	2.889	3.674	4.459	4.962
12	2.889	3.705	4.553	5.024
13	2.889	3.831	4.553	5.307
14	2.983	3.831	4.679	5.307
15	3.046	3.894	4.962	5.464

C.9 Calculation of Average Mass Transfer Coefficient With Distance at Different Flow Rate ($K_{avg} \times 10^5$ m^2/s)

Section	Distance covered	L/D_e	Flow rate (lit/min)			
			3.25	5.8	8.2	14.65
1	0-1	0.296	3.297	3.894	4.867	5.652
2	1-2	0.592	3.219	3.894	4.758	5.574
3	2-3	0.888	3.151	3.863	4.669	5.506
4	3-4	1.183	3.109	3.855	4.671	5.464
5	4-5	1.479	3.084	3.831	4.629	5.426
6	5-9	2.663	2.952	3.433	4.079	4.860
7	9-13	3.846	2.865	3.254	3.850	4.621
8	13-17	5.030	2.819	3.140	3.724	4.494
9	17-21	6.213	2.805	3.068	3.647	4.467
10	21-25	7.396	2.796	3.023	3.603	4.405
11	25-26	7.692	2.800	3.048	3.635	4.427
12	26-27	7.988	2.803	3.073	3.669	4.449
13	27-28	8.284	2.806	3.100	3.701	4.480
14	28-29	8.580	2.812	3.125	3.735	4.508
15	29-30	8.876	2.820	3.151	3.776	4.540

C.10   Calculation of Overall Mass Transfer Coefficient

Gas flowrate V_g (lit/min)	Superficial gas velocity u_g (m/s)	i_L	Reynolds number (Re)	Sherwood number (Sh)	K_g 10^5 (m/s)
1.65	0.013	59.24	392.93	1343.01	2.0463
3.25	0.025	82.73	755.65	1875.54	2.8577
5.80	0.044	95.91	1329.95	2174.36	3.3130
8.20	0.062	109.30	1874.02	2477.90	3.7755
11.50	0.087	133.18	2629.68	3019.29	4.6004
14.65	0.112	142.42	3385.32	3228.72	4.9195

APPENDIX   D

CURRENT-VOLTAGE DATA AND CALCULATED RESULTS

FOR SIMULTANEOUS GAS LIQUID FLOW

D.1   Liquid Flowrate = 4.4 lit/min
          Gas Flowrate = 5.0 lit/min

Current distribution at different cathode sections (mA)

Cathode Section	Applied Voltage(mV) 300	400	500	600	700	800
1	25	29	40	55	58	64
2	20	22	40	49	53	61
3	16	22	33	46	49	61
4	16	24	33	46	49	62
5	16	24	30	45	47	58
6	60	84	129	175	189	232
7	60	80	132	180	194	235
8	60	85	132	180	194	230
9	67	92	140	190	205	240
10	67	95	140	190	212	241
11	18	24	38	48	50	62
12	18	29	36	48	53	65
13	21	29	44	55	53	65
14	26	32	47	61	59	70
15	29	37	49	70	62	70
Total Measured Current, mA	540	775	1105	1455	1530	1845
Total Current Accounted, mA	540	708	1063	1440	1527	1816

D.2   Liquid Flowrate = 4.4 lit/min

        Gas Flowrate = 8.2 lit/min

Current distribution at different cathode sections (mA)

Cathode Section	Applied Voltage, mV 300	400	500	600	700	800
1	17	28	43	64	69	70
2	14	23	36	57	69	68
3	11	23	36	57	58	68
4	15	21	39	50	53	68
5	15	23	33	55	53	63
6	54	90	140	220	221	250
7	57	92	140	220	232	255
8	57	92	145	225	249	261
9	60	95	147	230	255	266
10	61	98	147	235	260	272
11	15	24	44	62	58	69
12	12	25	44	62	64	70
13	16	25	49	62	68	72
14	17	28	55	65	75	74
15	21	33	55	73	80	75
Total Measured Current, mA	545	890	1235	1765	1900	2010
Total current Accounted, mA	442	720	1153	1737	1864	2001

D.3   Liquid Flowrate = 6.1 lit/min

Gas Flowrate = 5.0 lit/min

Current distribution at different cathode sections (mA)

Cathode Section	Applied Voltage, mV	300	400	500	600	700	800
1		14	16	30	47	47	56
2		11	14	24	44	47	51
3		9	15	24	44	46	51
4		8	15	24	41	45	48
5		8	14	21	41	44	48
6		29	55	95	165	173	190
7		36	56	90	165	177	195
8		36	52	96	171	177	199
9		39	55	98	172	180	192
10		41	54	101	172	182	207
11		10	15	25	43	46	54
12		15	16	28	45	46	59
13		15	16	32	45	49	62
14		16	20	37	47	48	67
15		17	24	41	47	54	69
Total Measured Current, mA		390	550	895	1335	1400	1650
Total Current Accounted, mA		304	437	766	1289	1361	1548

D.4   Liquid Flowrate = 6.1 lit/min

Gas Flowrate = 8.2 lit/min

Current distribution at different cathode sections (mA)

Cathode Section	Applied Voltage, mV	300	400	500	600	700	800
1		14	35	55	55	61	78
2		14	35	51	48	54	74
3		14	28	51	52	54	73
4		12	29	51	53	57	73
5		12	29	49	53	54	72
6		44	114	190	204	215	290
7		49	111	195	204	221	290
8		50	115	190	209	225	295
9		51	115	196	209	228	295
10		51	120	210	215	228	298
11		14	30	55	51	58	75
12		14	30	55	57	56	78
13		17	32	63	60	61	70
14		17	33	68	63	65	81
15		20	36	70	67	74	83
Total Measured Current, mA		5000	1085	1600	1660	1805	2370
Total Current Accounted, mA		393	892	1549	1600	1711	2235

D.5   Liquid flow rate = 7.8 litre/min
       Gas flow rate =5.0 litre/min

Current distribution at different cathode section

Cathode Section	Applied Voltage (mV)	300	400	500	600	700	800
1		11	16	27	49	49	—
2		11	13	22	45	49	
3		8	12	25	40	44	
4		7	10	21	40	40	
5		7	12	21	40	40	
6		28	48	80	157	160	
7		30	49	85	162	165	
8		30	49	92	162	165	
9		31	52	92	165	171	
10		33	56	90	169	172	
11		9	14	22	43	46	
12		9	14	24	47	46	
13		11	17	24	48	54	
14		11	21	29	52	58	
15		11	25	29	55	65	
Total current measured(mA)		300	490	765	1300	1370	
Total current accounted (mA)		247	408	683	1274	1325	

D.6   Liquid flow rate = 7.8 litre/min
      Gas flow rate =5.0 litre/min

Current distribution at different cathode section

Cathode Section	Applied Voltage (mV)	300	400	500	600	700	800
1		9	24	35	48	53	66
2		8.5	21	32	48	53	64
3		8	21	29	43	52	63
4		8	20	29	44	52	63
5		10	20	28	41	52	60
6		33	80	114	162	205	242
7		33	76	117	165	205	245
8		34	81	120	169	209	245
9		35	83	128	175	208	251
10		32	85	128	178	211	251
11		7	22	33	45	51	67
12		9.5	22	36	53	54	67
13		11	26	41	59	54	72
14		12	27	41	58	57	78
15		12	31	45	60	60	83
Total current measured(mA)		300	705	1095	1395	1630	2045
Total current accounted (mA)		262	639	956	1348	1575	1917

Table D.7   Calculated results

Flowrates (lit/min)		Superficial velocities (m/s)		$\dfrac{U_g^{0.4}}{U_l^{0.2}}$	Limiting current i_L	Mass transfer coefficient
Liquid	Gas	U_l	U_g		(A/m^2)	(m/s)
4.4	5.0	0.033	0.038	0.535	48.06	1.66
4.4	8.2	0.033	0.062	0.651	58.19	2.01
6.1	5.0	0.046	0.038	0.500	44.06	1.53
6.1	8.2	0.046	0.062	0.609	52.69	1.82
7.8	5.0	0.059	0.038	0.476	42.85	1.48
7.8	6.5	0.059	0.046	0.527	46.03	1.59

D.8   Bubble size calculation

Liquid flowrate = 6.2 lit/min
Gas flowrate = 5.0 lit/min

Differential area chosen = 41.16 cm^2

Differential volume = 82.32 cm^3

Bubble diameter (inch)	Number of bubble
0.40	1
0.3	5
0.25	11
0.20	11
0.10	21

$$d_B = \frac{\Sigma nd^3}{\Sigma nd^2} = \frac{1\ \ 0.4^3 + 5\ \ 0.3^3 + 11\ \ 0.2^3 + 21\ \ 0.1^3}{1\ \ 0.4^2 + 5\ \ 0.3^2 + 11\ \ 0.25^2 + 11\ \ 0.2^2 + 21\ \ 0.1^2}$$

$$= \frac{0.4799}{1.9475} = 0.2464'' = 0.626\ cm = 6.26\ mm.$$

$$V_B = \frac{\pi}{6}\ \Sigma\ nd^3 = \frac{\pi}{6}\ \ 0.4799 = 0.2513\ in^3 = 4.1177\ cm^3$$

Volume fraction of gas present = 0.0500

D.9 Bubble size data

Gas flowrate (lit/min)	Liquid flowrate (lit/min)	Bubble diameter (inch)	No. of bubble
8.20		0.60	1
		0.30	3
		0.20	3
		0.15	6
		0.10	9
14.65		0.50	1
		0.30	4
		0.25	1
		0.20	5
		0.10	7
8.20	4.40	0.35	4
		0.25	11
		0.20	8
		0.10	7
		0.05	2

D.10 Calculation of standard deviation of bubble diameter

	Gas flowrate (litre/min)	Liquid flow rate (litre/min)	Average bubble diameter (mm)	Standard deviation
1.	8.20	-	9.12	0.0481
2.	14.65	-	7.97	0.0383
3.	5.00	6.20	6.26	0.0149
4.	8.20	4.40	6.71	0.0185